Guerit, L., et al., 2019, Fluvial landscape evolution controlled by the sediment deposition coefficient: Estimation from experimental and natural landscapes: Geology, https://doi.org/10.1130/G46356.1

GSA DATA REPOSITORY TEXT

Guerit et al., Fluvial landscape evolution controlled by the sediment deposition coefficient: estimation from experimental and natural landscapes

Laboratory setups and typical evolution of the experimental landscapes

Experimental landscapes show strong similarities with their natural equivalents and experimental drainage networks often follow geometric laws deduced from natural systems (Schumm et al., 1987; Bonnet and Crave, 2006; Bonnet, 2009; Graveleau et al., 2015; Viaplana-Muzas et al., 2015; 2018). In particular, the drainage networks of experimental landscapes often show a clear power-law relationship between the slopes of the streams and the catchment areas (Lague et al, 2003; Guerit et al., 2018, Moussirou and Bonnet, 2018). This suggests that the stream power incision model is a good first-order description of such landscape dynamics. Perfect downscaling of such experiments is not possible because of scale distortion when downscaling natural conditions to the lab. In that sense, geomorphic laboratory models are not analog but experimental. However, they have shown to be a powerful tool to study the dynamics of natural landscapes (Paola et al., 2009).

Two sets of experiments are analyzed in this study (Babault et al, 2005; Rohais, 2007; Rohais et al, 2012). Both setups are composed by a rectangular box filled with a saturated granular material and where erosion occurs. In Rohais et al.'s experiments, this box is 320 x 200-mm wide and 500-mm deep while in Babault et al.'s work, the box is 400 x 600-mm wide and 500-mm deep. Its base can move upward or downward to simulate uplift, and its motion is driven by a screw and a computer-controlled stepping motor. The experiments analyzed here are performed with a vertical motion of 5 to 20 mm/h.

The experimental material is obtained by mixing silica powder (D50 = 10-20 μm) with water (20% in weight of the silica powder). The mixture is homogenized to saturate the porosity of the silica paste and to reduce infiltration phenomena. The mixture is loaded in the erosion box and at the beginning of a run, the surface of the erosion box is flat. This material is then uplifted and eroded by surface runoff, and it has been successfully used to simulate natural continental landscapes (Bonnet and Crave, 2006; Bonnet, 2009; Moussirou and Bonnet, 2018).

Water is delivered by four sprinklers located at the edges of the experimental domain. The experiments analyzed here are performed with precipitation rate of 40 to 130 mm/h and drops are small enough (<0.5 mm) to avoid splash dispersion on the surface of the model, reducing the impact of hillslope diffusion. During DEMs acquisitions, uplift and rainfall are stopped.

In the setup used by Rohais (Rohais, 2007; Rohais et al., 2012), the erosion box is coupled to a deposition box with dimensions of 600 x 1000 mm and a depth of 500 mm. The two boxes are linked through a small 20-mm long, 20-mm large and 500-mm deep opening, which is equivalent to a coupling point between a catchment and a fan in natural systems. As a consequence, in this setup, a single catchment coupled to a unique alluvial fan develop. The deposition box is covered by a lid to prevent complex interactions between the rain and the river flow. During an experiment, landscape dissection initiates at the outlet of the erosion box and propagates upward. A ramified drainage network develops on the surface of the erosion box and the catchment eventually reaches a dynamic steady-state. The material eroded in the catchment is deposited within the second box and gradually built an alluvial fan. The area and the slope of the fan increase rapidly at the beginning of an experiment, and they then

observe a continuous but slower increase in area and in slope. Eventually, the slope stabilizes and a very slow increase in area at constant slope can be observed. Experiments are run until the fan reaches the edges of the box.

In the setup used by Babault et al. (2005), the erosion box is surrounded by a 500-mm wide (P1) or 150-mm wide (P2) plateau. When the erosion box starts to be uplifted, landscape erosion initiates at the edges of this box and propagates upward into the box. The average elevation of the uplifted landscape increases and eventually stabilizes when the erosion box reaches a dynamic steady-state. In this setup, outlets are not imposed and multiple catchments form. Eroded sediments can then be deposited on the plateau where they built alluvial fans that eventually coalesce and form a bajada. Fans then grow at a constant slope until they reach the edges of the deposition plateau. As they increase in length, the apex must aggrade to keep the slope constant. As they reach the edges, a final phase of aggradation is observed. The fan slope increases up to a threshold where the sediment flux is eventually totally bypassed. The catchments reach steady-state only after the fans stop aggrading.

The landscapes analyzed in this study correspond to the steady-state phases of the experiments.

Apparent ζ in natural landscapes

The scaling factors ζ deduced from the slopes of the rivers closed to the apexes in natural landscapes seem to be overestimated, as it leads to unrealistically low settling velocities. This overestimation might be related to the temporal dynamics of landscape evolution, which occurs mostly when it rains, i.e. only during a fraction of time. In fact, for a given period of

time, the average time variation of elevation h is the variation when there is a topographic change (when it rains or when there is transport) multiplied by the fraction of time χ during which this variation occurs:

$$\frac{\partial' h}{\partial t} = \chi \frac{\partial h}{\partial t}, (1)$$

where the bar denotes the time average.

During the periods of topographic changes, we have:

$$\frac{\partial' h}{\partial t} = \chi \frac{\partial h}{\partial t}, (1)$$

where $\frac{\partial h}{\partial t}=D-D$ is the deposition rate and D is the detachment rate. Equation (2) can be recast as:

where $\frac{\partial h}{\partial t}=-\nabla q_s$ is the sediment flux per unit of width and $q_s$is the water flux per unit of width.

Defining the time averaged quantities $\overline{q_w}$ and $q_w' = \chi q_w$, Equation (3) now reads:

$$q_s' = \chi q_s$$

Combining this equation with the time averaged topographic variation (Equation (1)), we have:

$$q_w' = \chi q_w$$

where $\frac{\partial h}{\partial t}=\frac{q_s'}{\zeta q_w}-\epsilon\left(\frac{q_w'}{\chi}\right), (4)$ is the apparent transport length, adapted to the mean water discharge $\frac{\partial h}{\partial t}=-\frac{\partial q_s}{\partial x}$, and Equation (5) is the equation solved in landscape evolution models. The physical transport length is ζ, but the one inferred from the DEMs and using an average precipitation rate is q_w'. Based on Equation (5), it thus appears that we overestimate the transport length by a factor χ. In consequence, if topographic changes occur 10% of the time ($\chi = $ ', the transport length inferred from the DEM is 10 times larger than the true value. In a very arid environment, if topographic changes only 1% of the time, $1/\chi$ would be overestimated by a

98 factor 100. Nonetheless, we should use γ=0.1 in landscape evolution models as they integrate
99 periods at rest and period with topographic evolutions. This overestimation due to the
100 frequency of rainfall is negligible in experimental landscapes because precipitation rate is
101 constant through time.
102
103 **REFERENCES CITED**

104 Babault, J., Bonnet, S., Crave, A., and Van Den Driessche, J., 2005, Influence of piedmont
105 sedimentation on erosion dynamics of an uplifting landscape: an experimental approach
106 Geology, v. 33, no. 4, p. 301–304.
107 Bonnet, S., 2009, Shrinking and splitting of drainage basins in orogenic landscapes from the
108 migration of the main drainage divide: Nature Geoscience, v. 2, no. 11, p. 766.
109 Bonnet, S., and Crave, A., 2006, Macroscale dynamics of experimental landscapes :
110 Geological Society, London, Special Publications, v. 253, no. 1, p. 327–339.
111 Graveleau, F., Strak, V., Dominguez, S., Malavieille, J., Chatton, M., Manighetti, I., and Petit,
112 C., 2015. Experimental modelling of tectonics–erosion–sedimentation interactions in
113 compressional, extensional, and strike–slip settings. Geomorphology v. 244, p. 146–168.
114 Guerit, L., Goren, L., Dominguez, S., Malavieille, J., and Castelltort, S., 2018, Landscape
115 'stress' and reorganization from χmaps: Insights from experimental drainage networks in
116 oblique collision setting: Earth Surface Processes and Landforms, vo. 43, no. 15, p.
117 3152–3163.
118 Lague, D., Crave, A., Davy, P., 2003, Laboratory experiments simulating the geomorphic
119 response to tectonic uplift: Journal of Geophysical Research, v. 108, no. B1, p. ETG 3-1–
120 ETG 3-20.

121 Moussirou, B., and Bonnet, S., 2018, Modulation of the erosion rate of an uplifting landscape
122 by long-term climate change: An experimental investigation: Geomorphology, v. 303, p.
123 456–466.
124 Paola, C., Straub, K., Mohrig, D., and Reinhardt, L., 2009, The “unreasonable effectiveness”
125 of stratigraphic and geomorphic experiments : Earth-Science Reviews, vo. 97, p. 1–43.
126 Rohais, S., 2007, Architecture stratigraphique et flux sédimentaires sur la marge sud du golfe
127 de Corinthe (Grèce) : Analyse de terrain, modélisations expérimentales et numériques
128 [Ph.D. thesis]: Université de Rennes 1, 386 p.
129 Rohais, S., Bonnet, S., and Echard, R., 2012, Sedimentary record of tectonic and climatic
130 erosional perturbations in an experimental coupled catchment-fan system: Basin
131 Research, v. 24, no. 2, p. 198–212.
132 Schumm, S., Mosley, M., and Weaver, W., 1987, Experimental fluvial geomorphology: New
133 York, John Wiley and Sons, 413 p.
134 Viaplana−Muzas, M., Babault, J., Dominguez, S., Van Den Driessche, J., and Legrand, X.,
135 2018, Modeling of drainage dynamics influence on sediment routing system in a fold−
136 and−thrust belt, Basin Research, doi:10.1111/bre.12321.
137 Viaplana−Muzas, M., Babault, J., Dominguez, S., Van Den Driessche, J., and Legrand, X.,
138 2015, Drainage network evolution and patterns of sedimentation in an experimental
139 wedge: Tectonophysics v. 664, p. 109–124.

GSA DATA REPOSITORY

Guerit et al., Fluvial landscape evolution controlled by the sediment deposition coefficient: estimation from experimental and natural landscapes

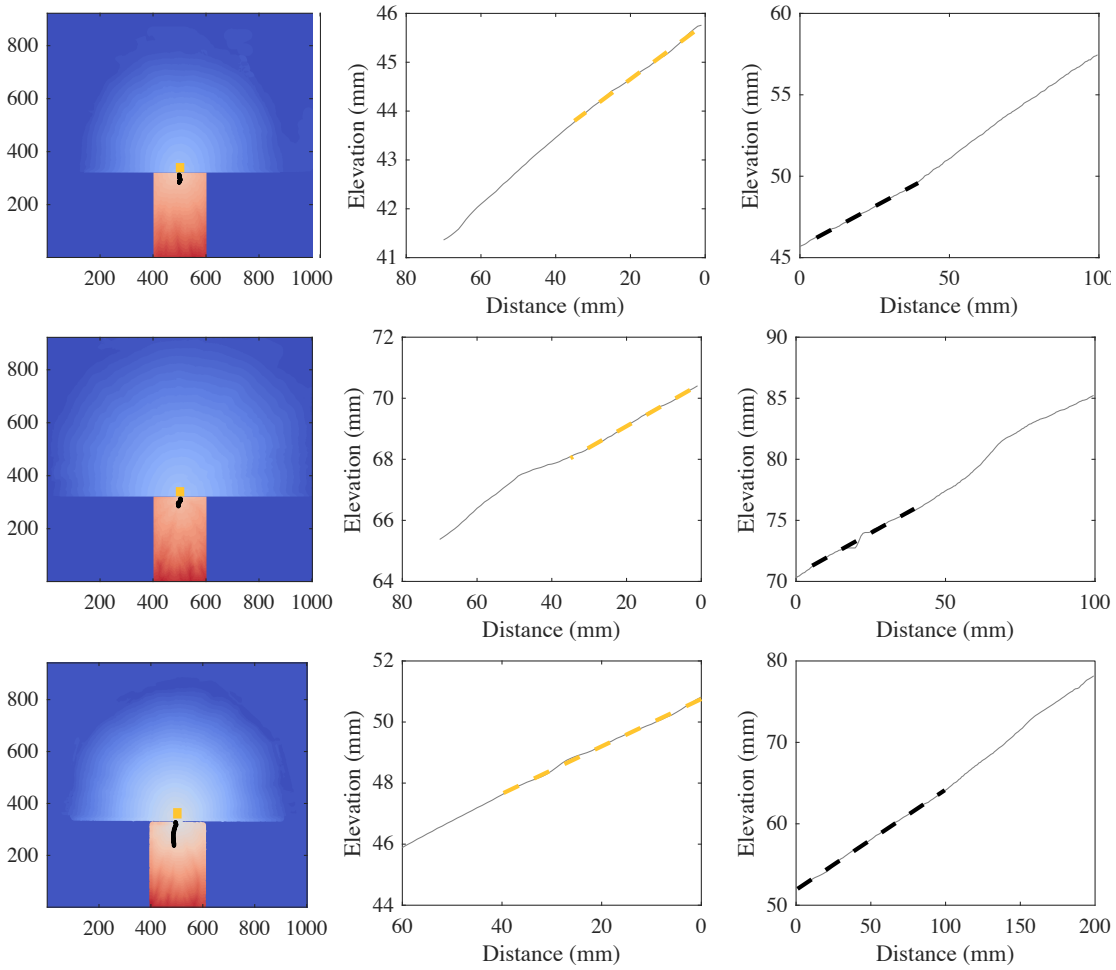

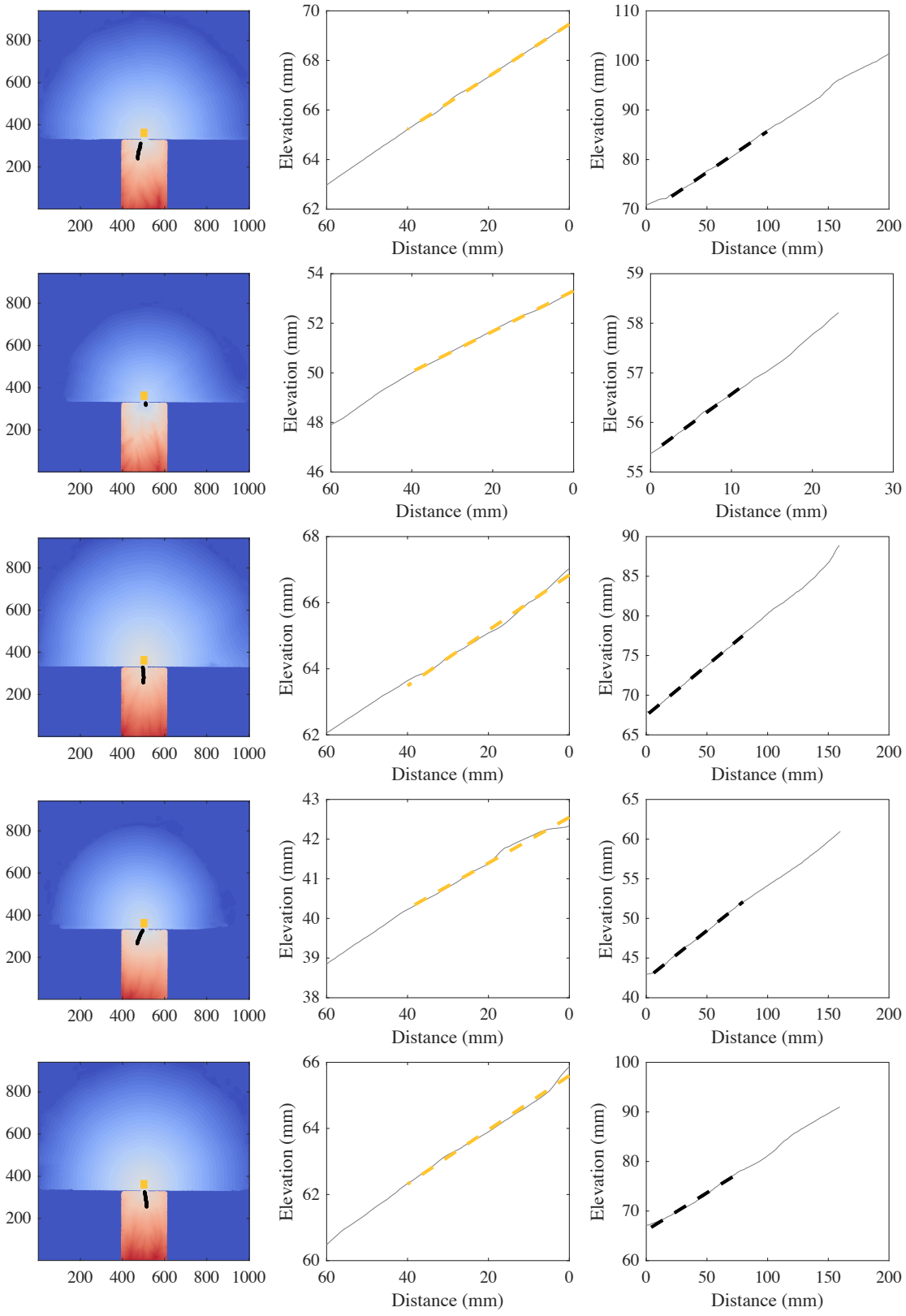
800
600
400
200
200 400 600 800 1000
Elevation (mm)
Distance (mm)
60 40 20 0
0 50 100 150 200
0 10 20 30

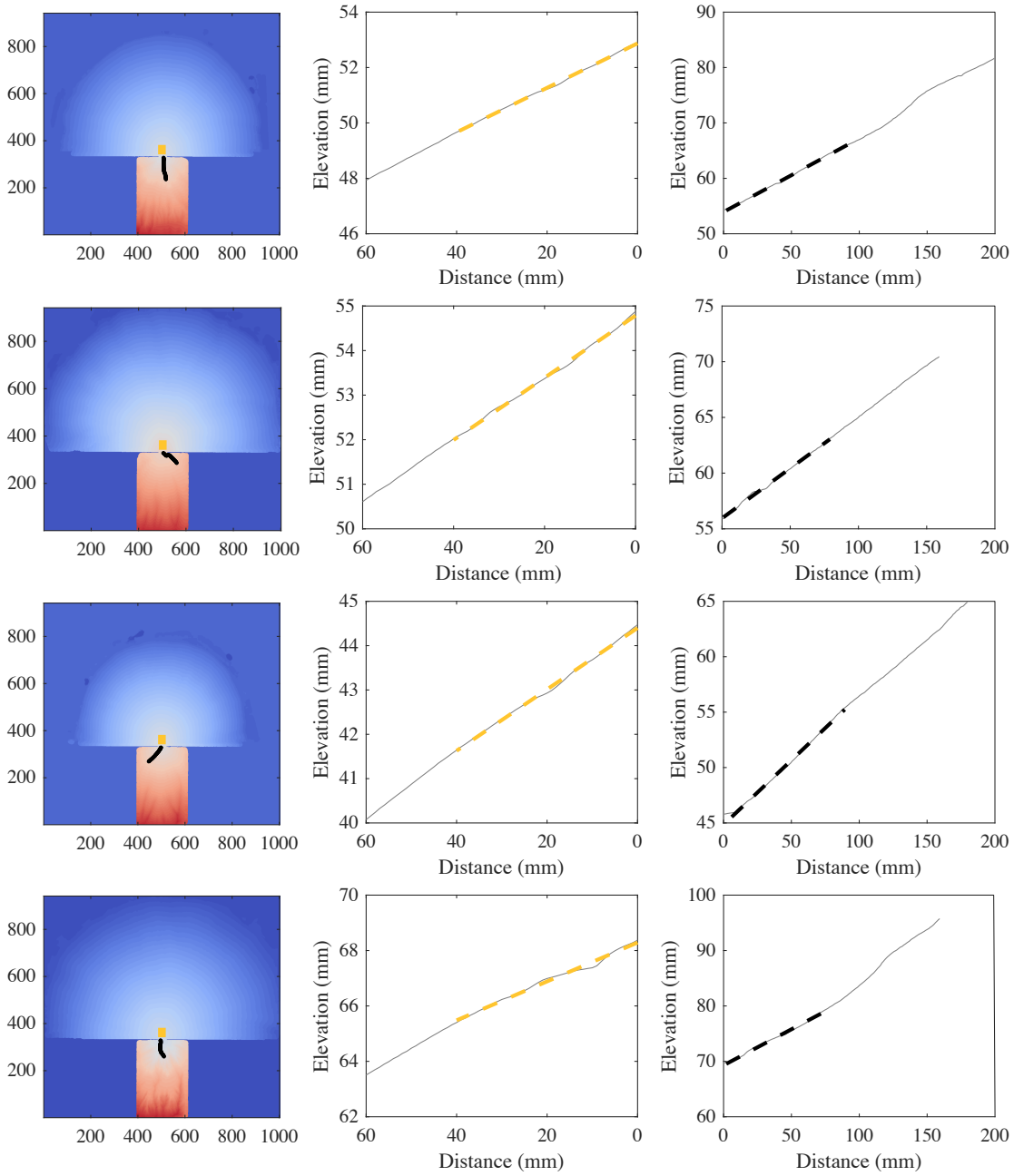

Figure DR1: Picture, Digital Elevation Models, and slope estimations of the 12 experiments from Rohais (2007) and Rohais et al. (2012). Grey line is the river profile close to the apex, dotted lines indicate the linear fit in the foreland (orange) and in the catchment (black).

References

Rohais: Architecture stratigraphique et flux sédimentaires sur la marge sud du golfe de Corinthe (Grèce) : Analyse de terrain, modélisations expérimentales et numériques, Ph.D. thesis, Université de Rennes 1, http://tel.archives-ouvertes.fr/tel-00154788, 2007.

Rohais, S., Bonnet, S., and Eschard, R.: Sedimentary record of tectonic and climatic erosional perturbations in an experimental coupled catchment-fan system, Basin Research, 24, 198–212, 2012.

GSA DATA REPOSITORY

Guerit et al., Fluvial landscape evolution controlled by the sediment deposition coefficient: estimation from experimental and natural landscapes

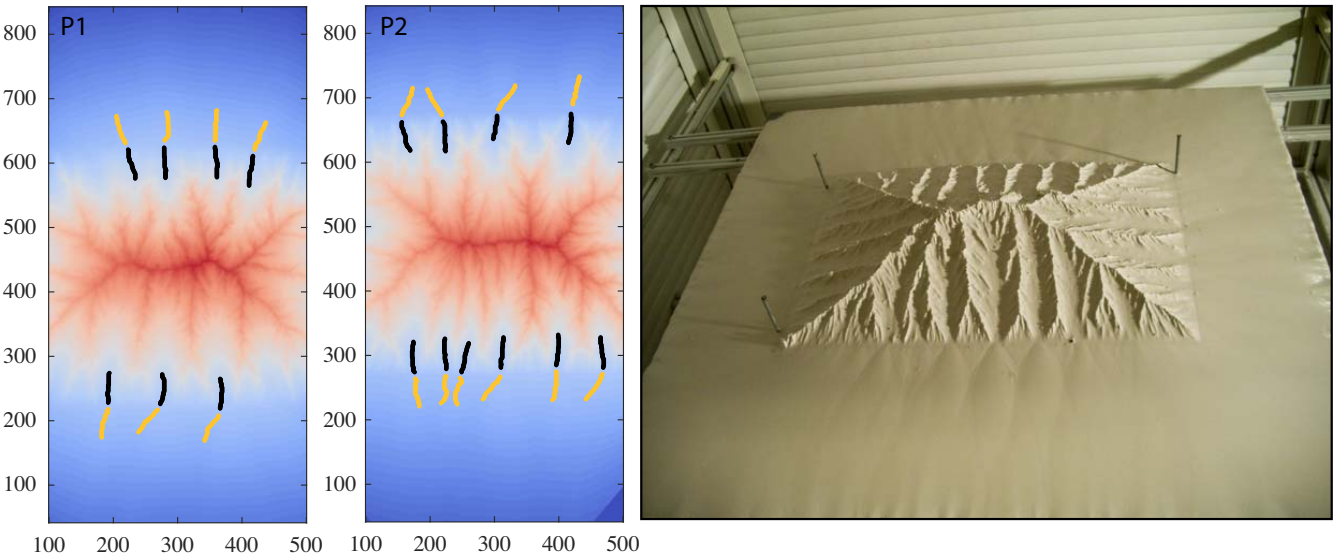

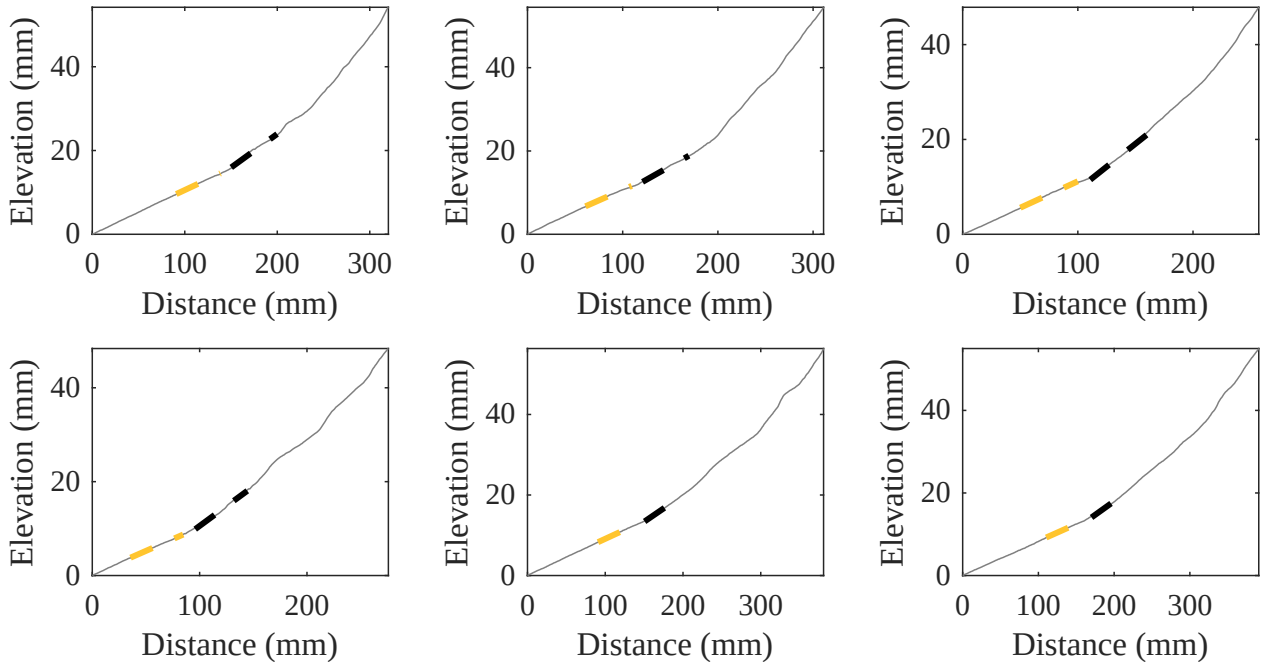

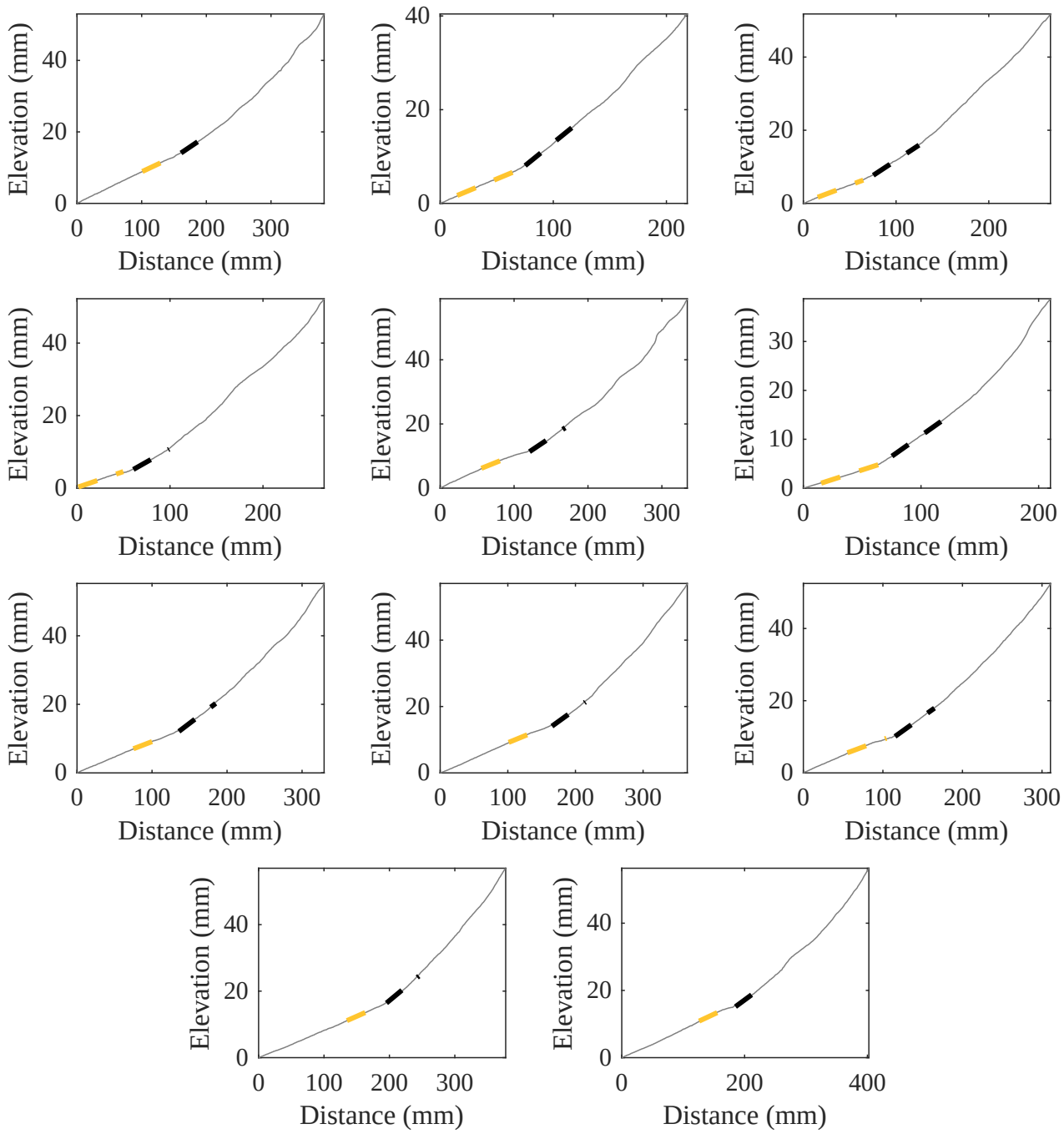

Figure DR2: Picture, Digital Elevation Models, and slope estimations of the 2 experiments from Babault et al. (2005). Grey line is the river profile close to the apex, dotted lines indicate the linear fit in the foreland (orange) and in the catchment (black).

References

Babault, J., Bonnet, S., Crave, A., and Van Den Driessche, J.: Influence of piedmont sedimentation on erosion dynamics of an uplifting landscape: an experimental approach, Geology, 33, 301–304, 2005.

GSA DATA REPOSITORY

Guerit et al., Fluvial landscape evolution controlled by the sediment deposition coefficient: estimation from experimental and natural landscapes

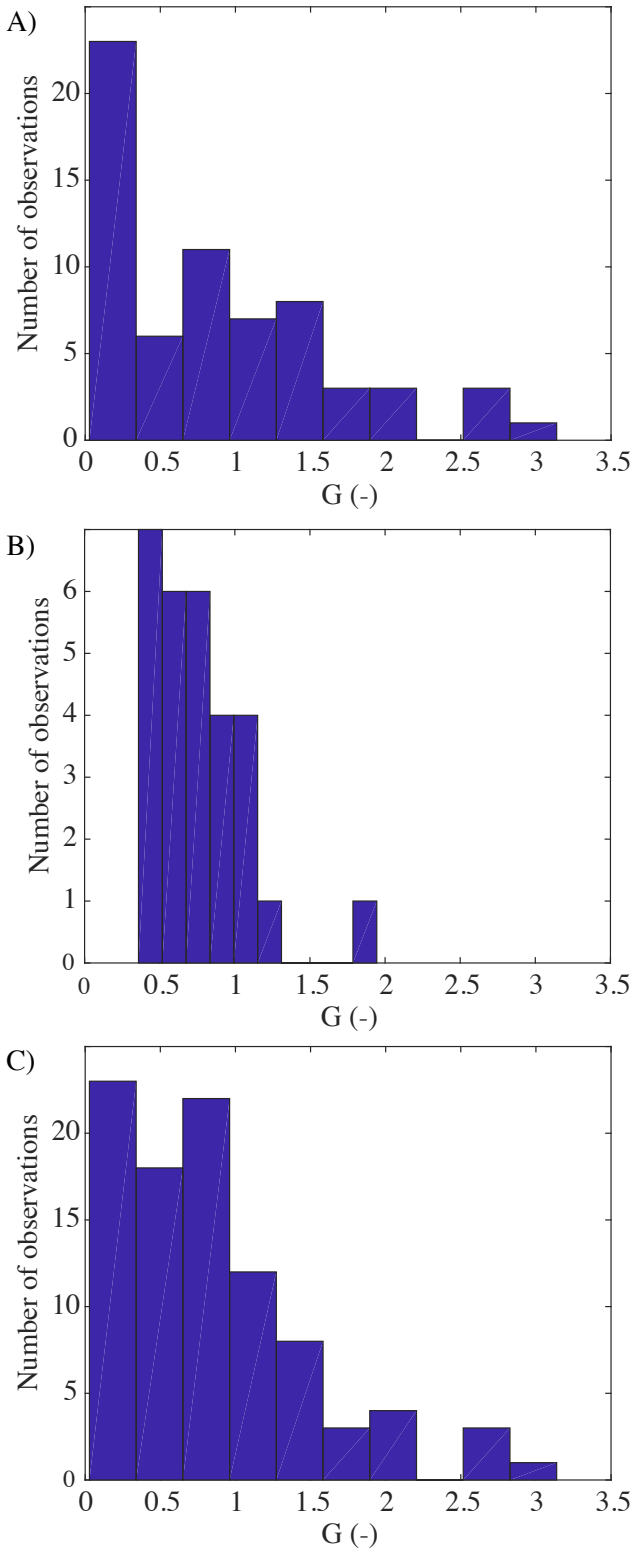

Figure DR3: Distributions of the estimated G values for A) the natural examples, B) the experimental examples, and C) all the data together.

GSA DATA REPOSITORY

Guerit et al., Fluvial landscape evolution controlled by the sediment deposition coefficient: estimation from experimental and natural landscapes

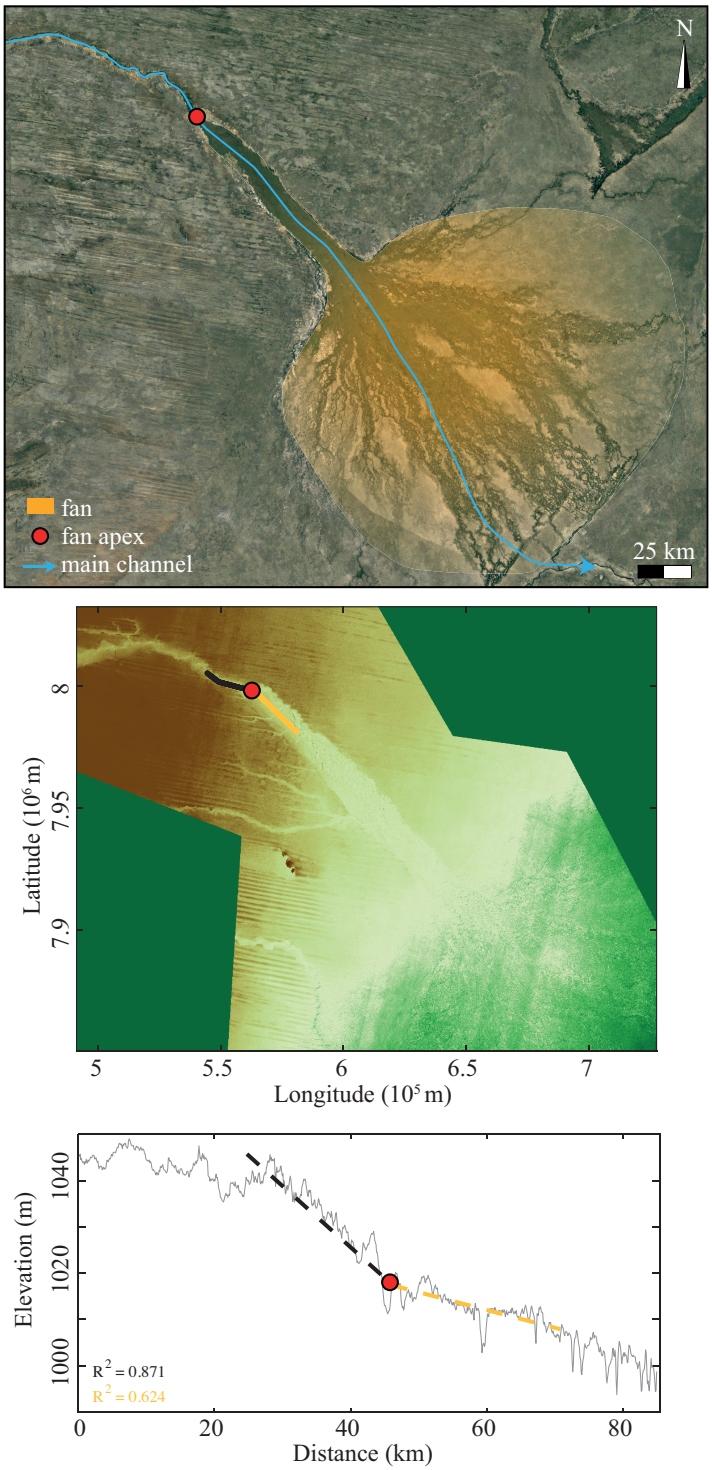

Figure DR4: Map, Digital Elevation Model and slope estimations of the catchment-fan system of the study site Okavango (see Table 2). Grey line is the river profile close to the apex (red dot), dotted lines indicate the linear fit in the foreland (orange) and in the catchment (black).

GSA DATA REPOSITORY

Guerit et al., Fluvial landscape evolution controlled by the sediment deposition coefficient: estimation from experimental and natural landscapes

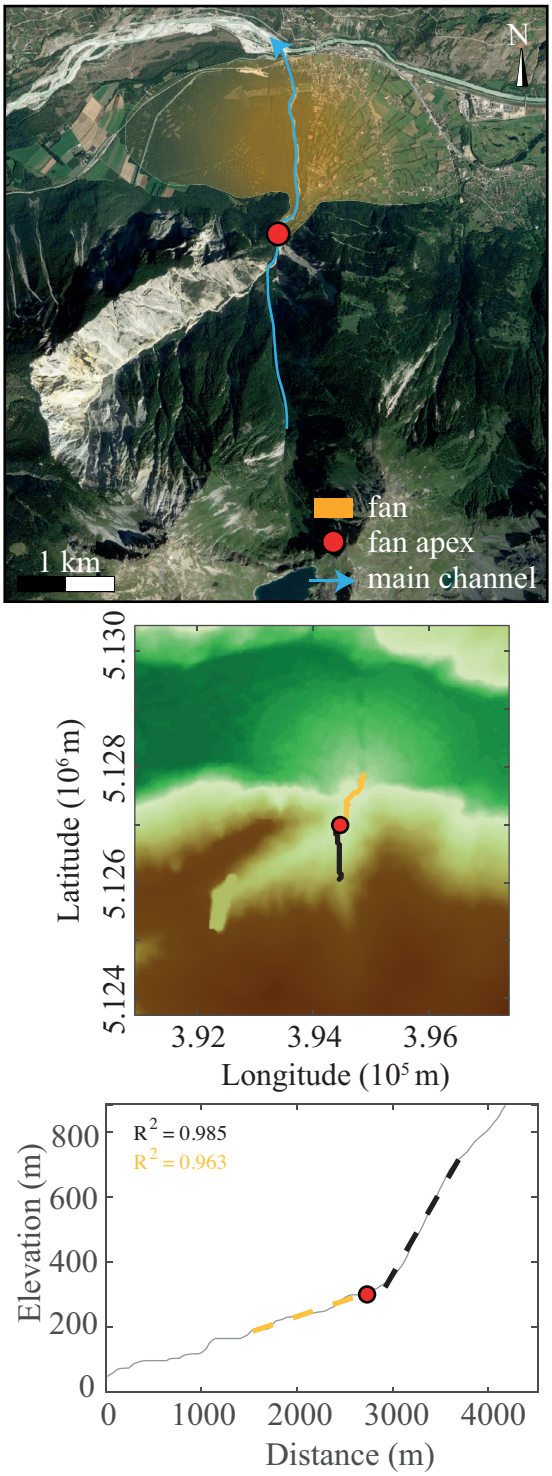

Figure DR5: Map, Digital Elevation Model and slope estimations of the catchment-fan system of the study site Illgraben (see Table 2). Grey line is the river profile close to the apex (red dot), dotted lines indicate the linear fit in the foreland (orange) and in the catchment (black).

GSA DATA REPOSITORY

Guerit et al., Fluvial landscape evolution controlled by the sediment deposition coefficient: estimation from experimental and natural landscapes

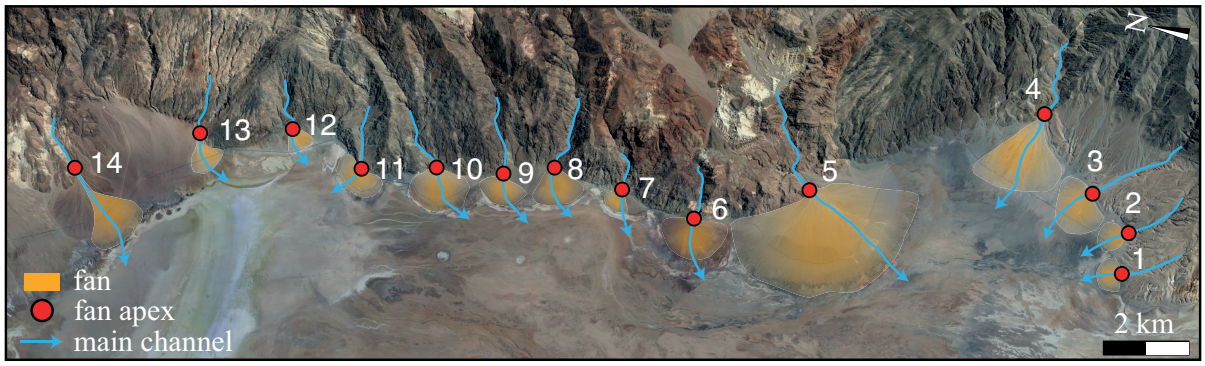

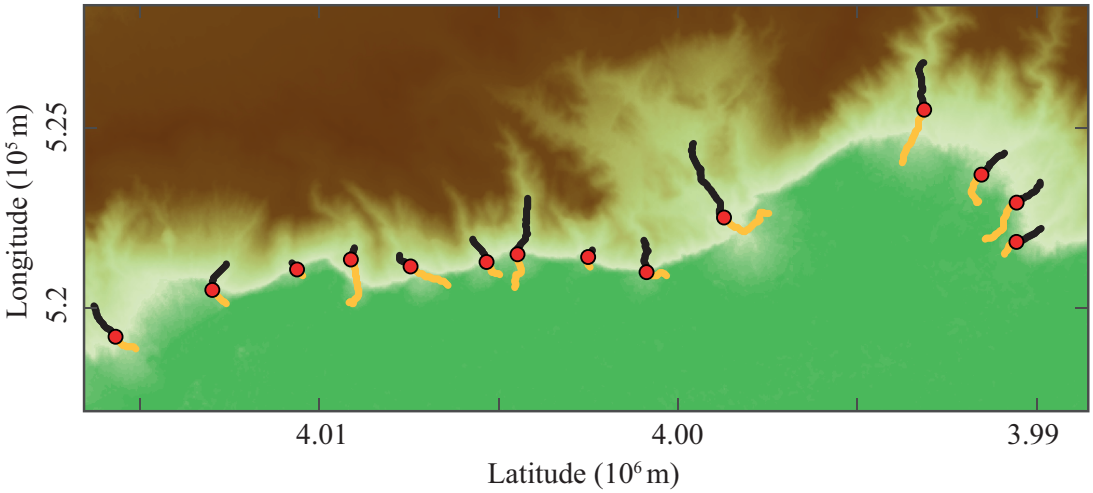

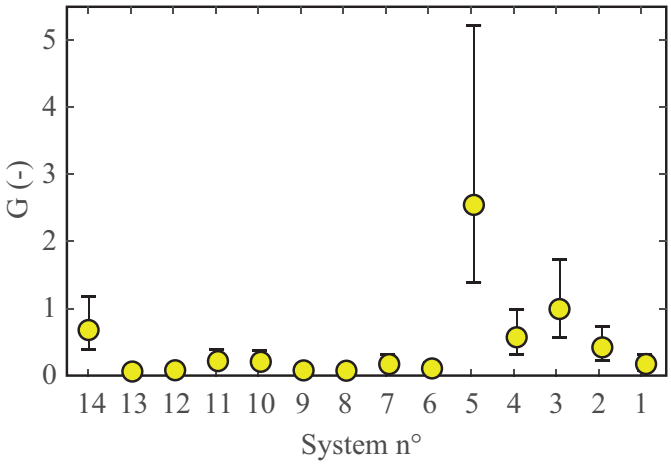

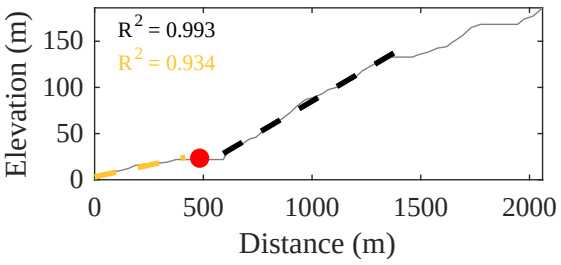

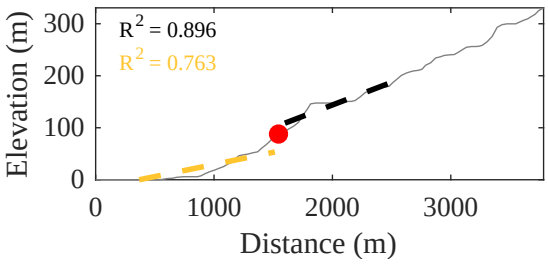

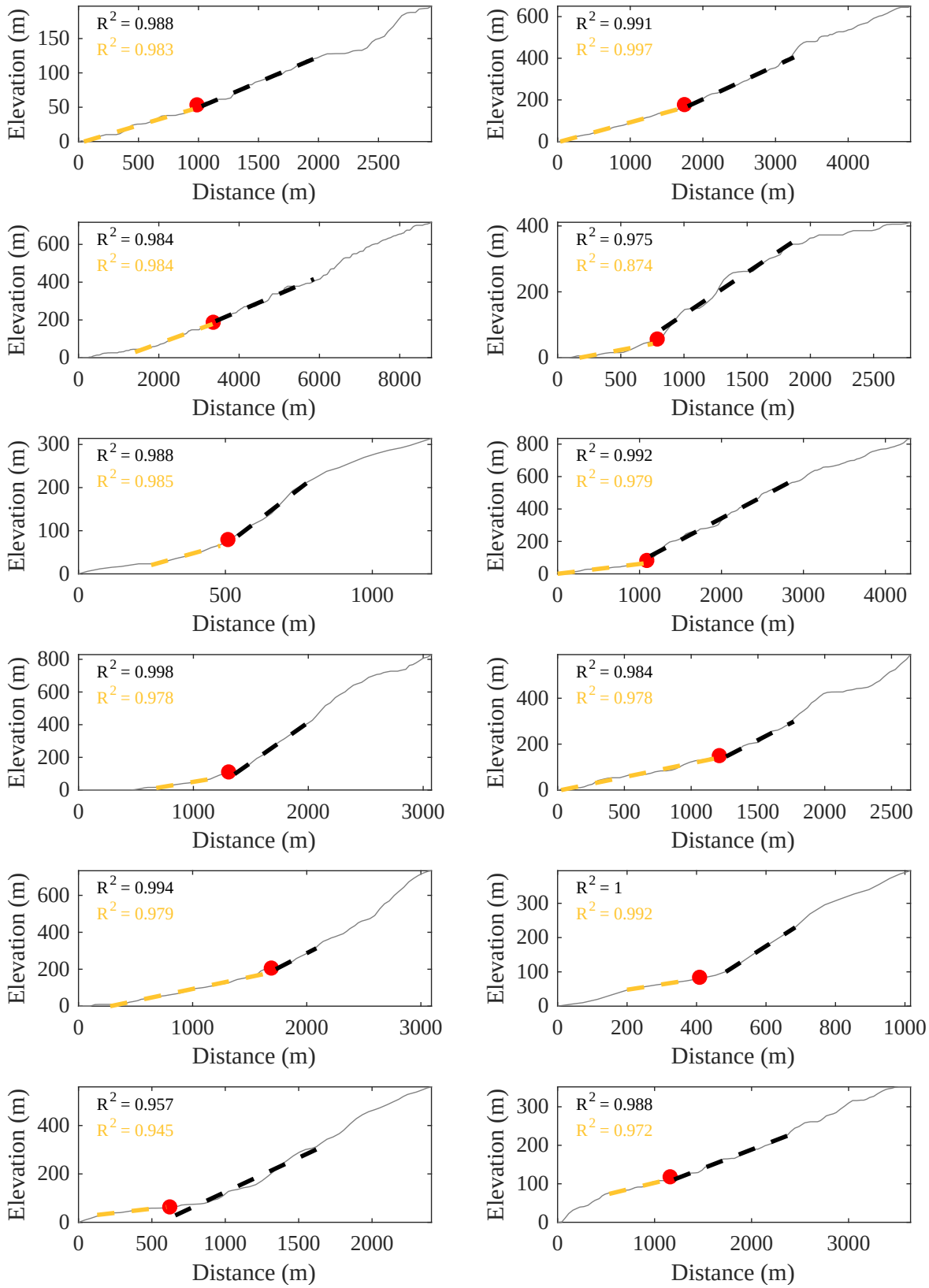

Figure DR6: Map, Digital Elevation Model and slope estimations of the 14 natural catchment-fan systems from the study site Death Valley (see Table 2). Grey line is the river profile close to the apex, dotted lines indicate the linear fit in the foreland (orange) and in the catchment (black).

GSA DATA REPOSITORY

Guerit et al., Fluvial landscape evolution controlled by the sediment deposition coefficient: estimation from experimental and natural landscapes

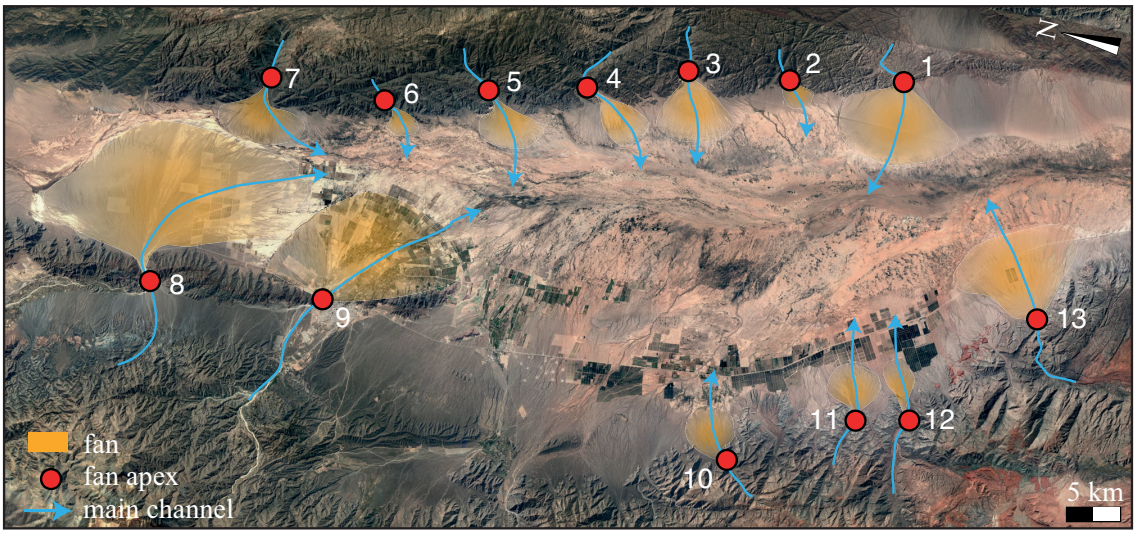

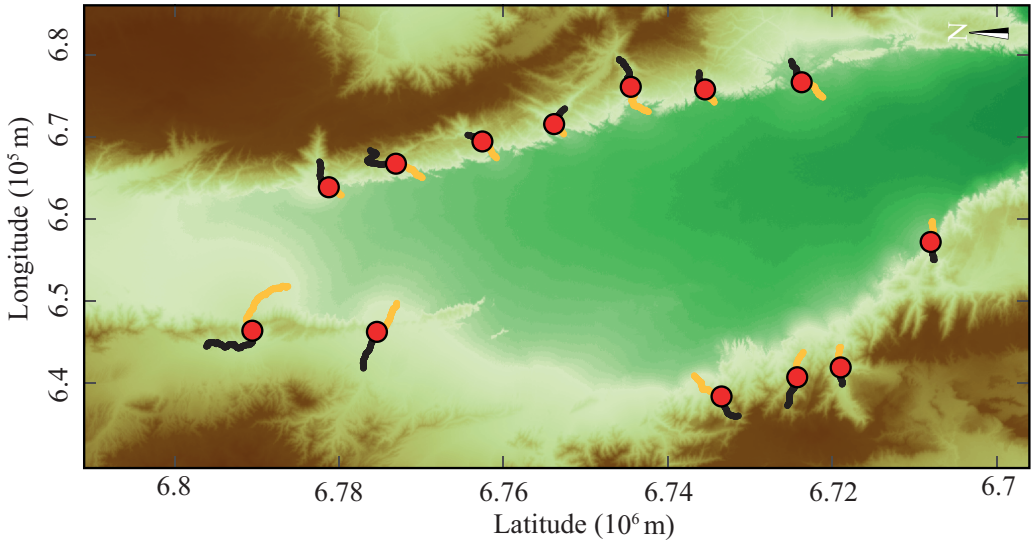

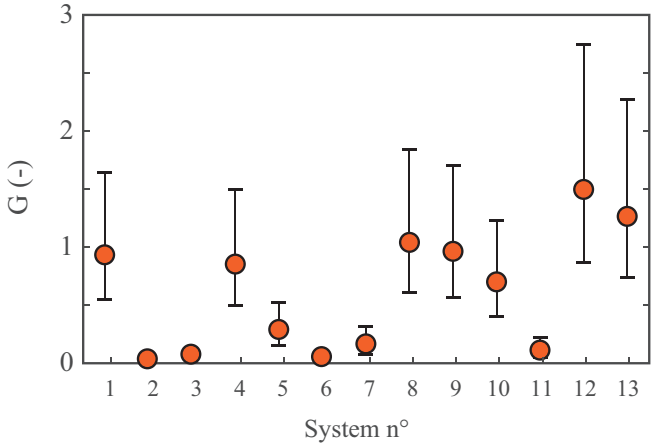

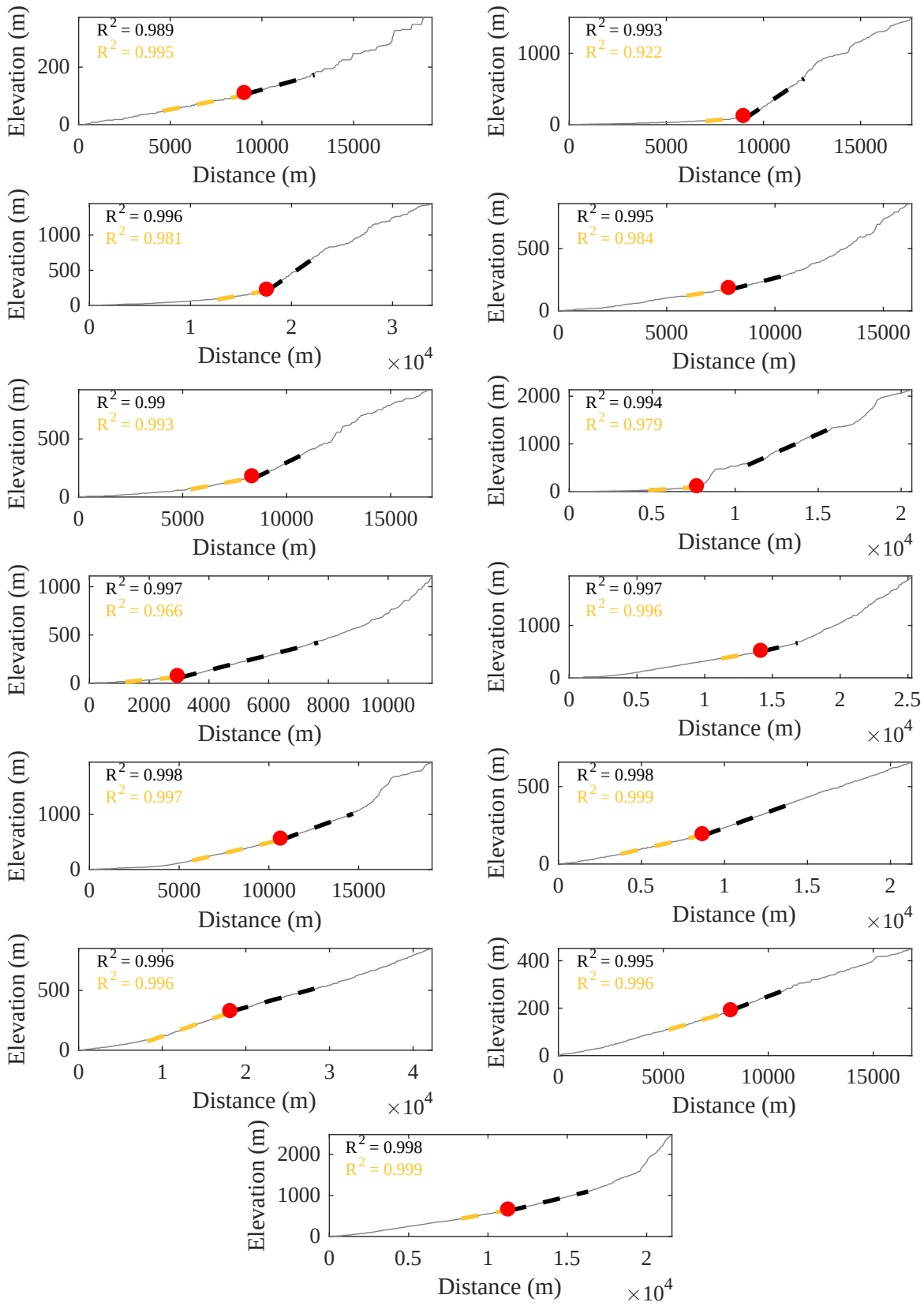

Figure DR7: Map, Digital Elevation Model and slope estimations of the 13 natural catchment-fan systems from the study site Andes 1 (see Table 2). Grey line is the river profile close to the apex, dotted lines indicate the linear fit in the foreland (orange) and in the catchment (black).

GSA DATA REPOSITORY

Guerit et al., Fluvial landscape evolution controlled by the sediment deposition coefficient: estimation from experimental and natural landscapes

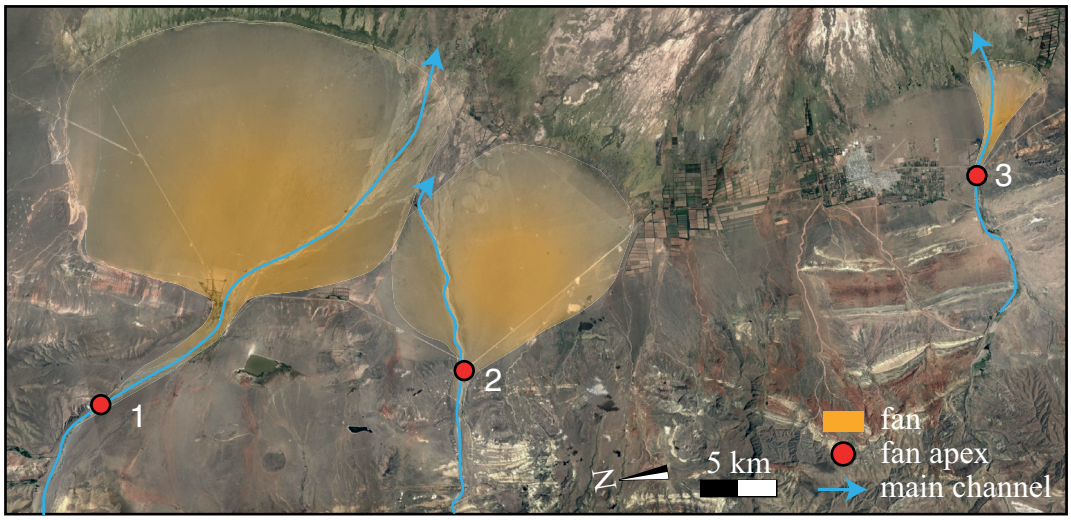

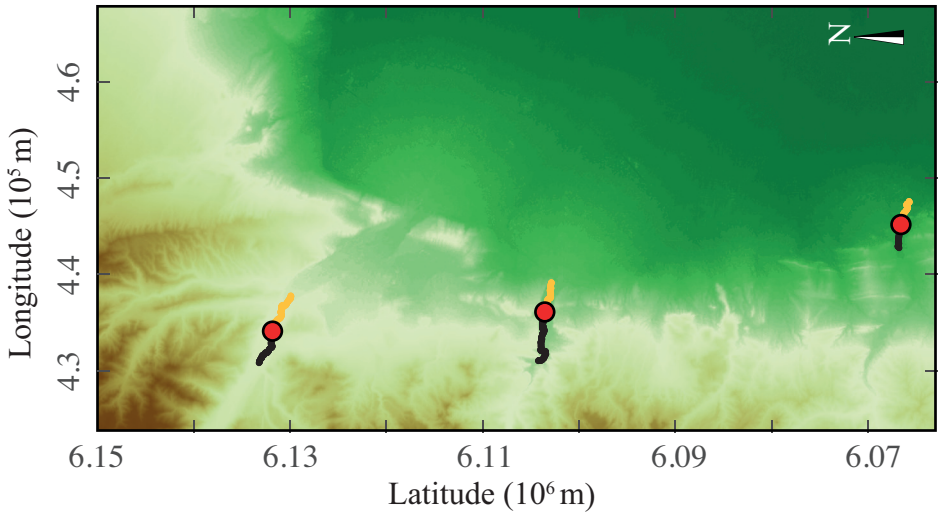

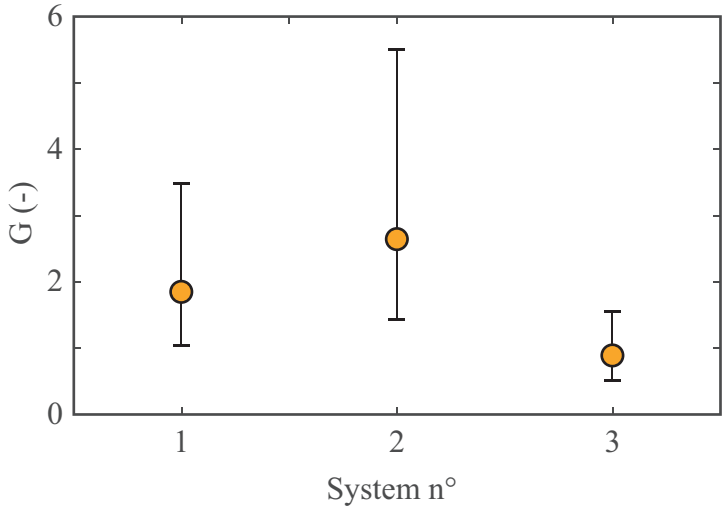

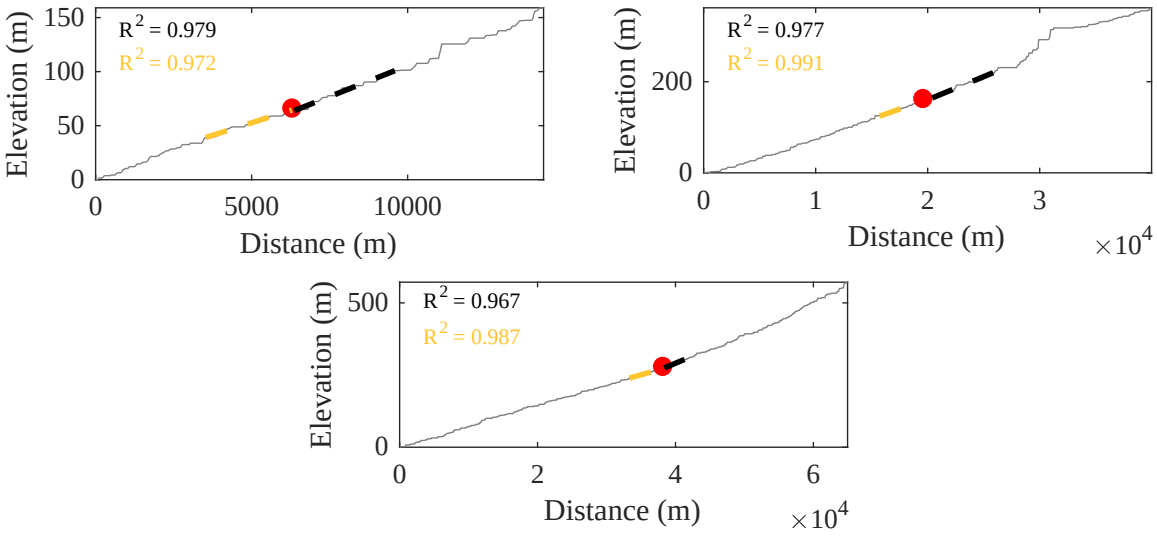

Figure DR8: Map, Digital Elevation Model and slope estimations of the 3 natural catchment-fan systems from the study site Andes 2 (see Table 2). Grey line is the river profile close to the apex, dotted lines indicate the linear fit in the foreland (orange) and in the catchment (black).

GSA DATA REPOSITORY

Guerit et al., Fluvial landscape evolution controlled by the sediment deposition coefficient: estimation from experimental and natural landscapes

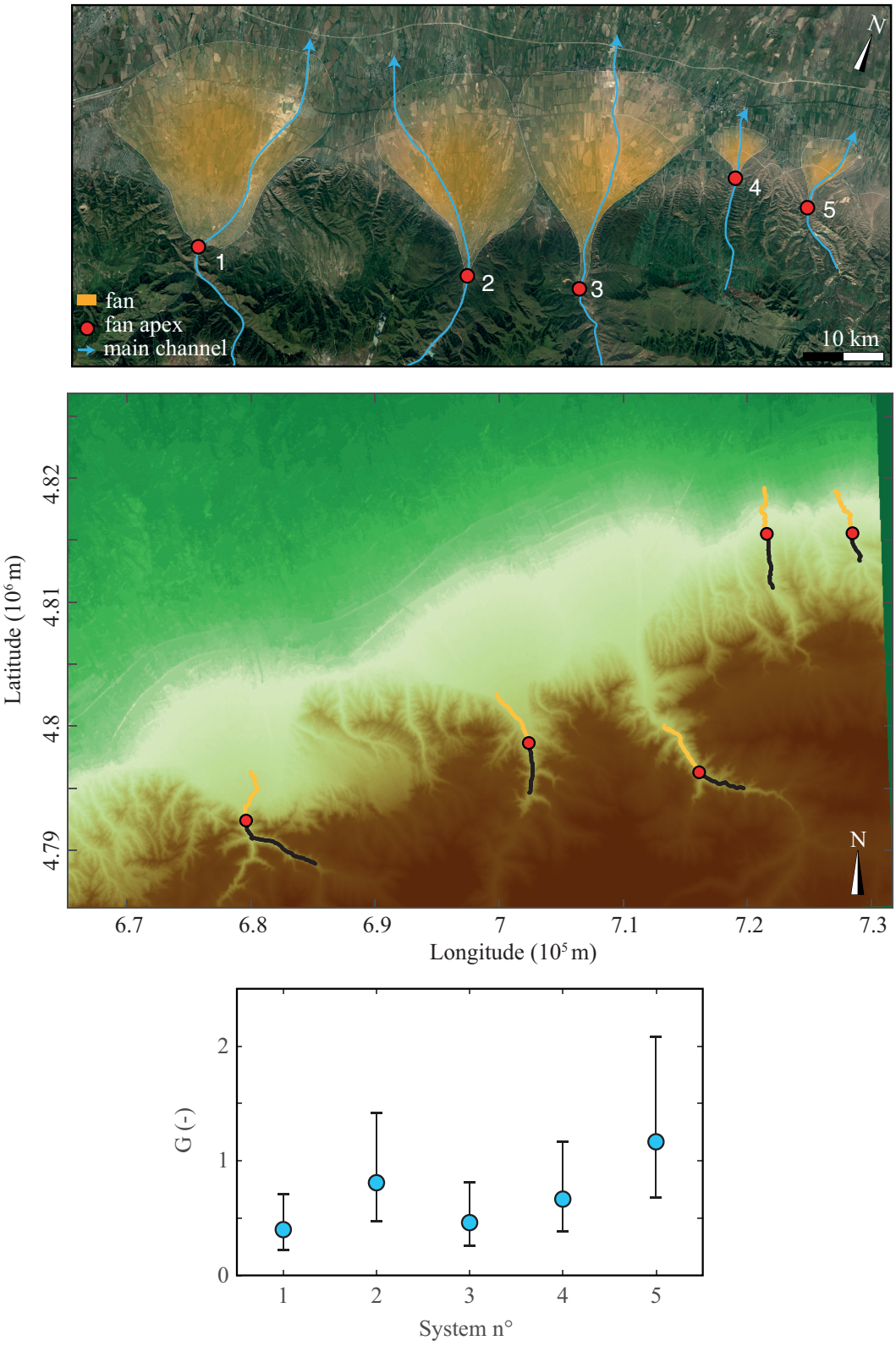

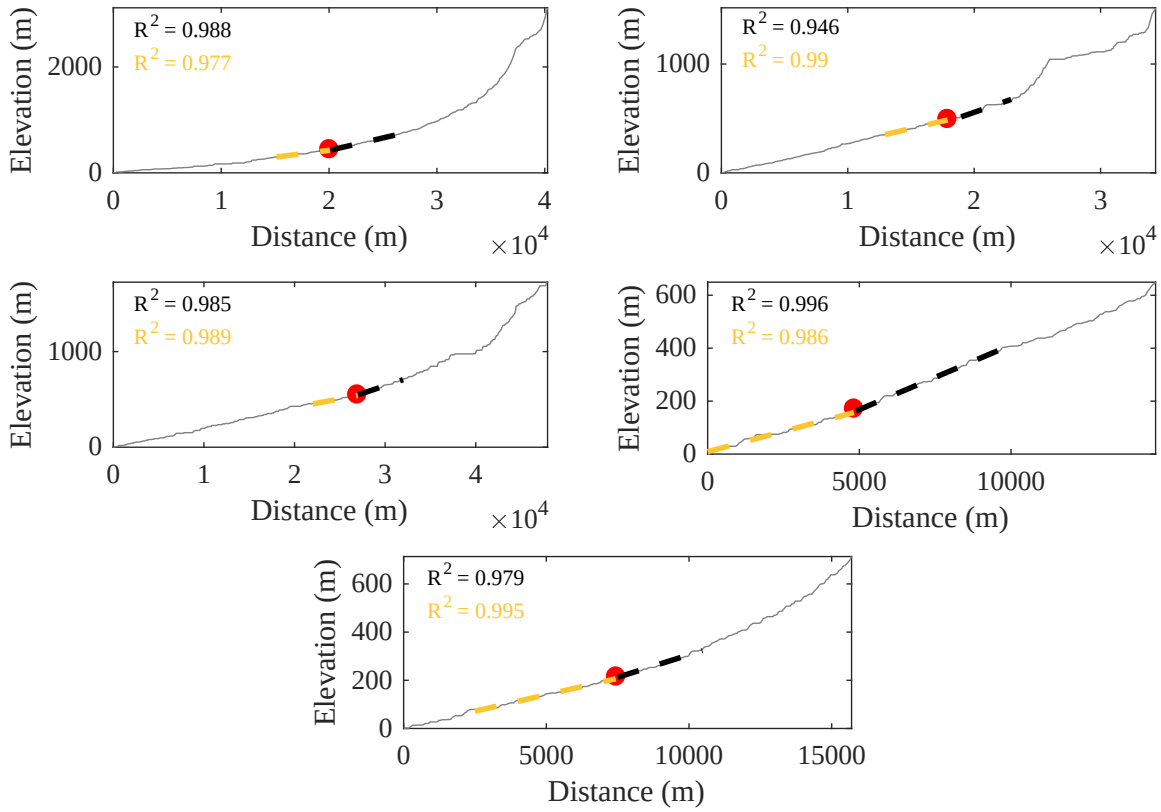

Figure DR9: Map, Digital Elevation Model and slope estimations of the 5 natural catchment-fan systems from the study site Tian Shan 1 (see Table 2). Grey line is the river profile close to the apex, dotted lines indicate the linear fit in the foreland (orange) and in the catchment (black).

GSA DATA REPOSITORY

Guerit et al., Fluvial landscape evolution controlled by the sediment deposition coefficient: estimation from experimental and natural landscapes

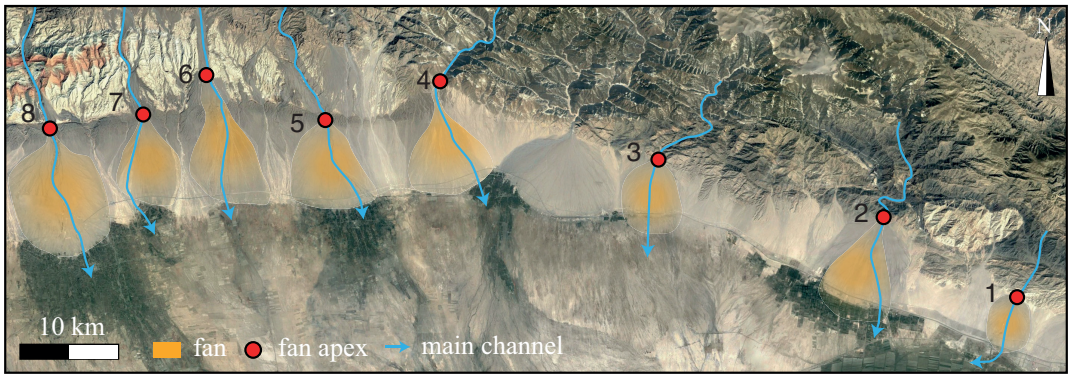

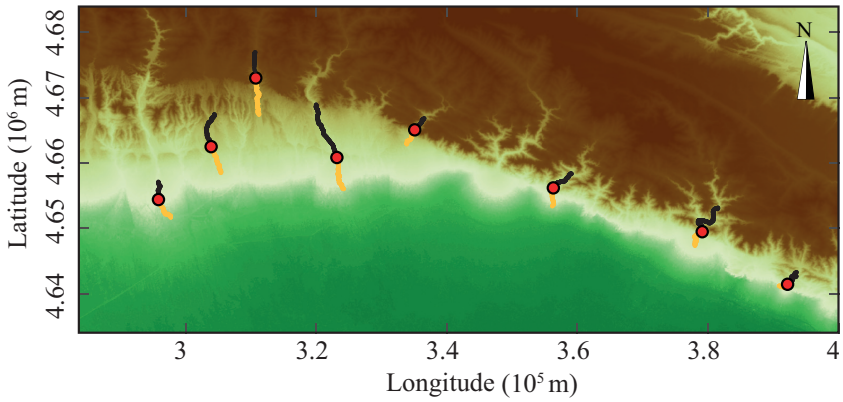

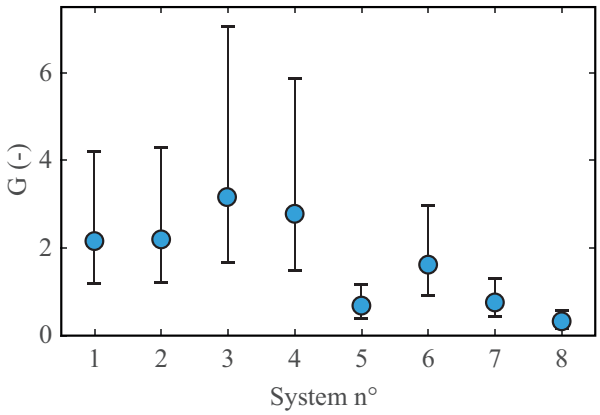

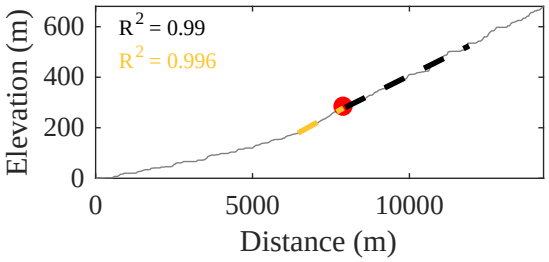

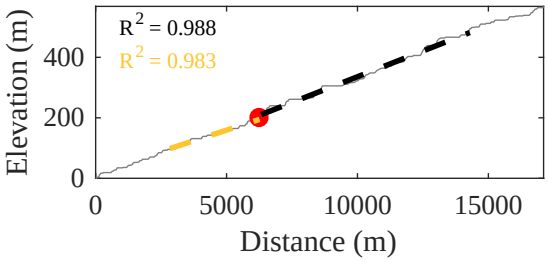

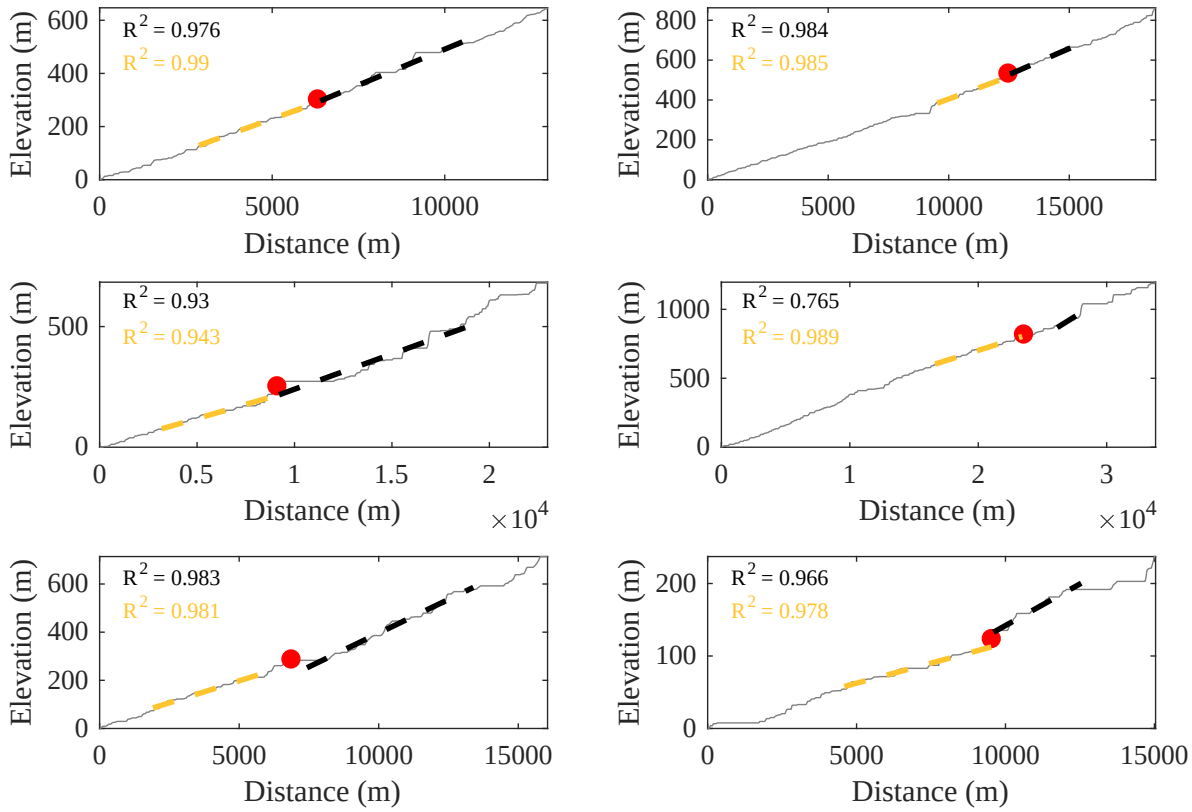

Figure DR10: Map, Digital Elevation Model and slope estimations of the 8 natural catchment-fan systems from the study site Tian Shan 2 (see Table 2). Grey line is the river profile close to the apex, dotted lines indicate the linear fit in the foreland (orange) and in the catchment (black).

GSA DATA REPOSITORY

Guerit et al., Fluvial landscape evolution controlled by the sediment deposition coefficient: estimation from experimental and natural landscapes

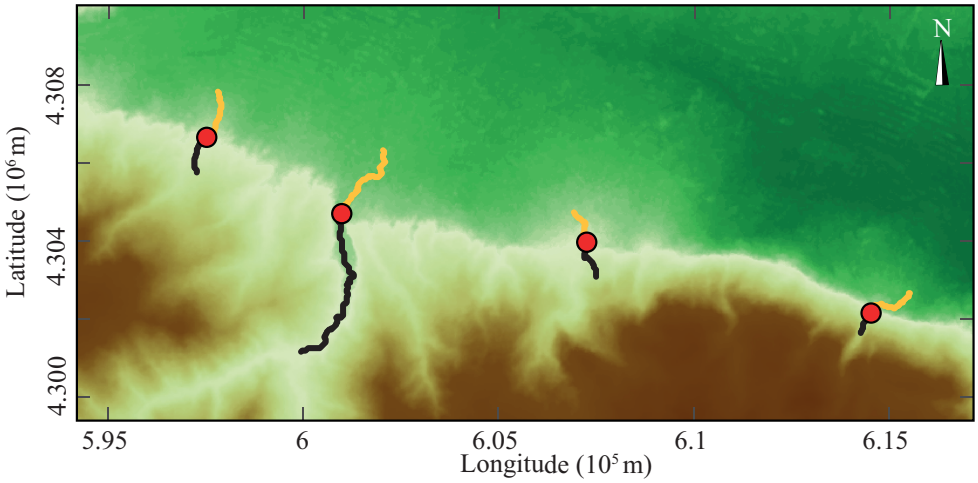

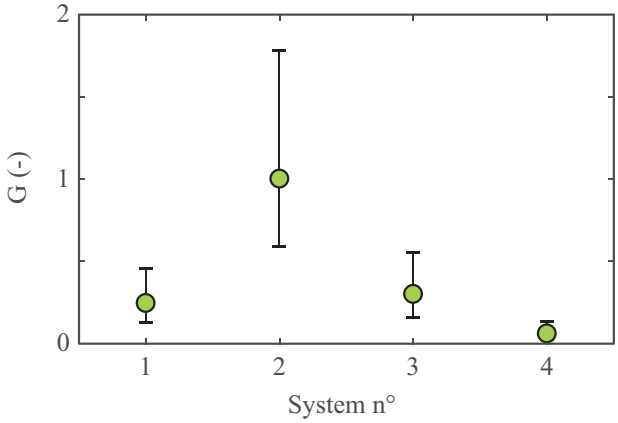

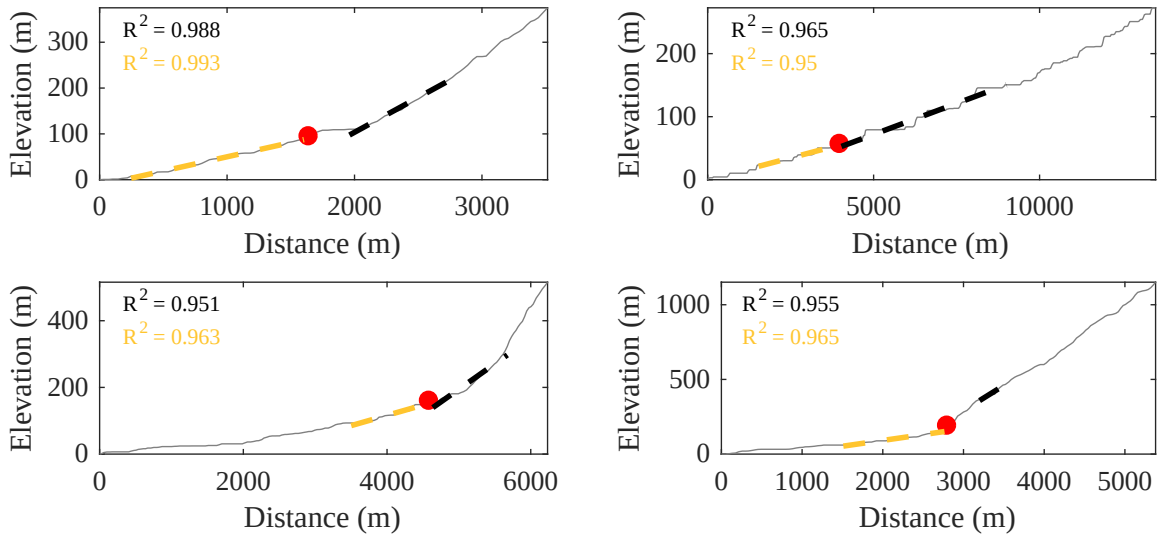

Figure DR11: Map, Digital Elevation Model and slope estimations of the 4 natural catchment-fan systems from the study site Pindus (see Table 2). Grey line is the river profile close to the apex, dotted lines indicate the linear fit in the foreland (orange) and in the catchment (black).

GSA DATA REPOSITORY

Guerit et al., Fluvial landscape evolution controlled by the sediment deposition coefficient: estimation from experimental and natural landscapes

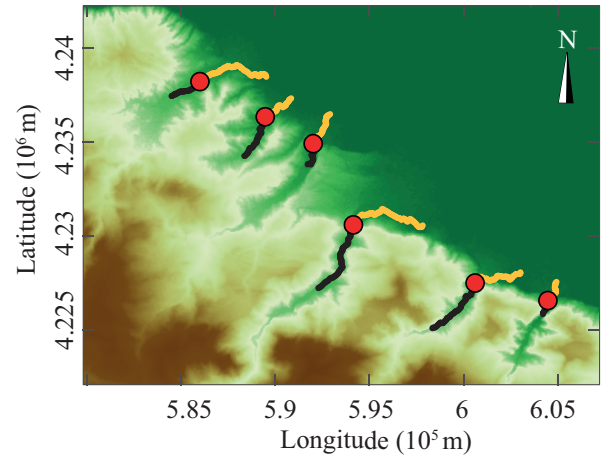

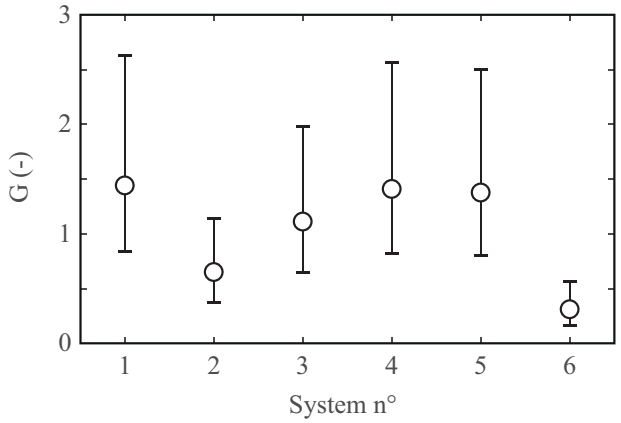

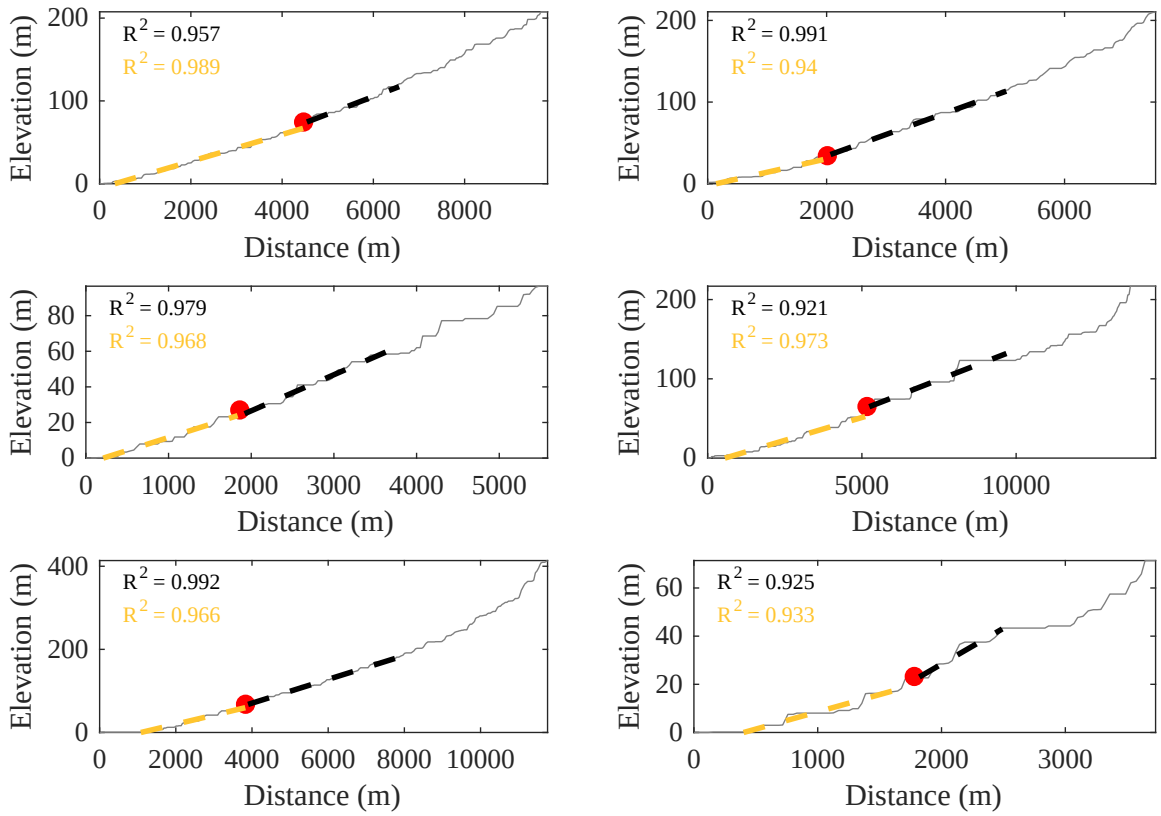

Figure DR12: Map, Digital Elevation Model and slope estimations of the 6 natural catchment-fan systems from the study site Corinth (see Table 2). Grey line is the river profile close to the apex, dotted lines indicate the linear fit in the foreland (orange) and in the catchment (black).

GSA DATA REPOSITORY

Guerit et al., Fluvial landscape evolution controlled by the sediment deposition coefficient: estimation from experimental and natural landscapes

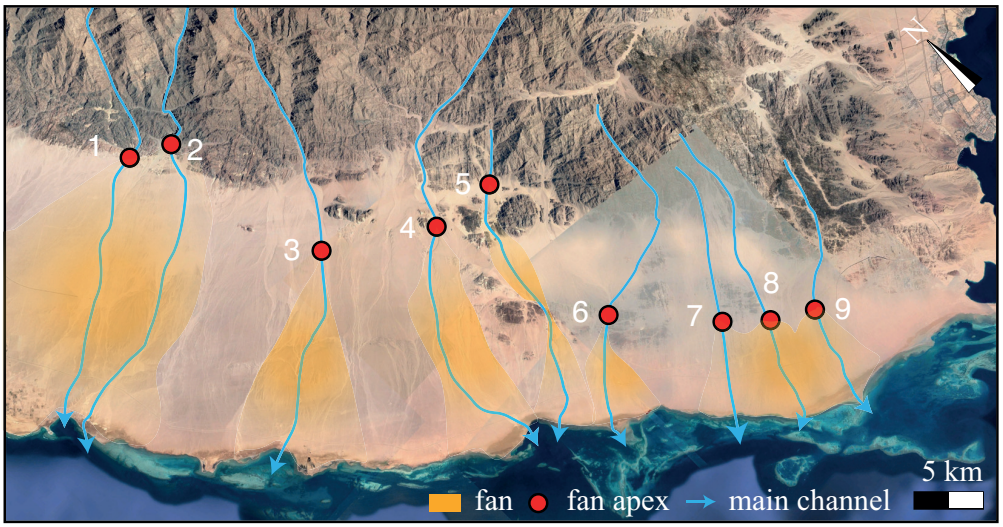

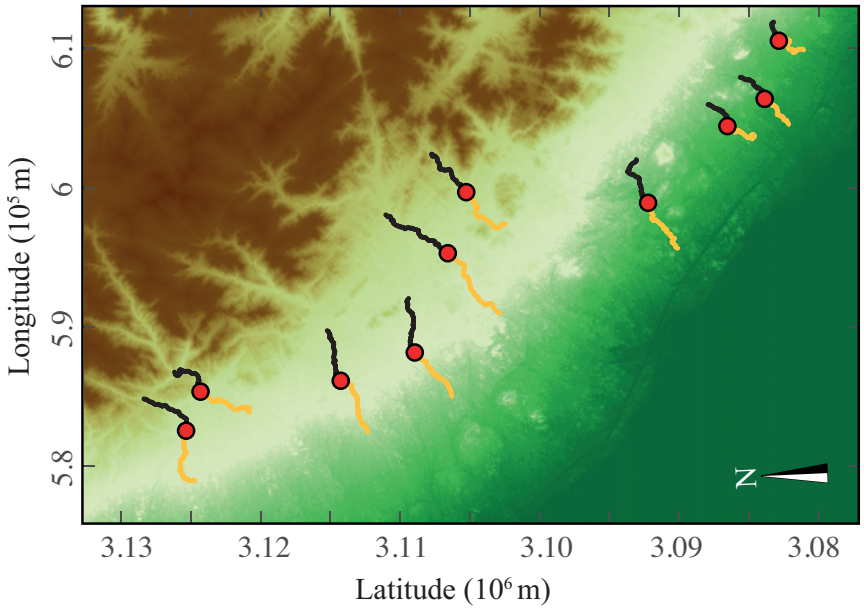

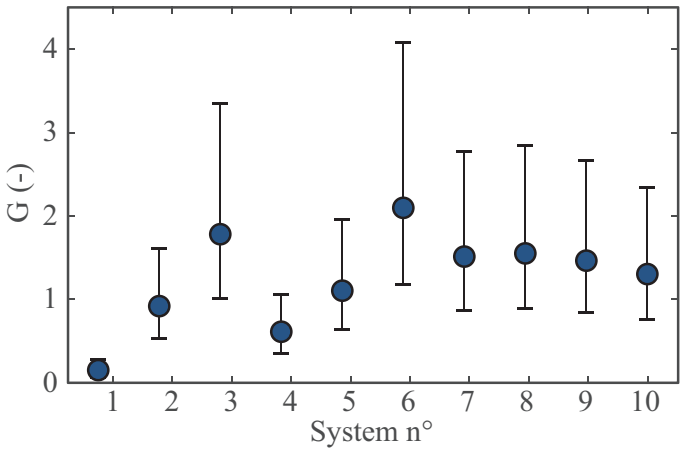

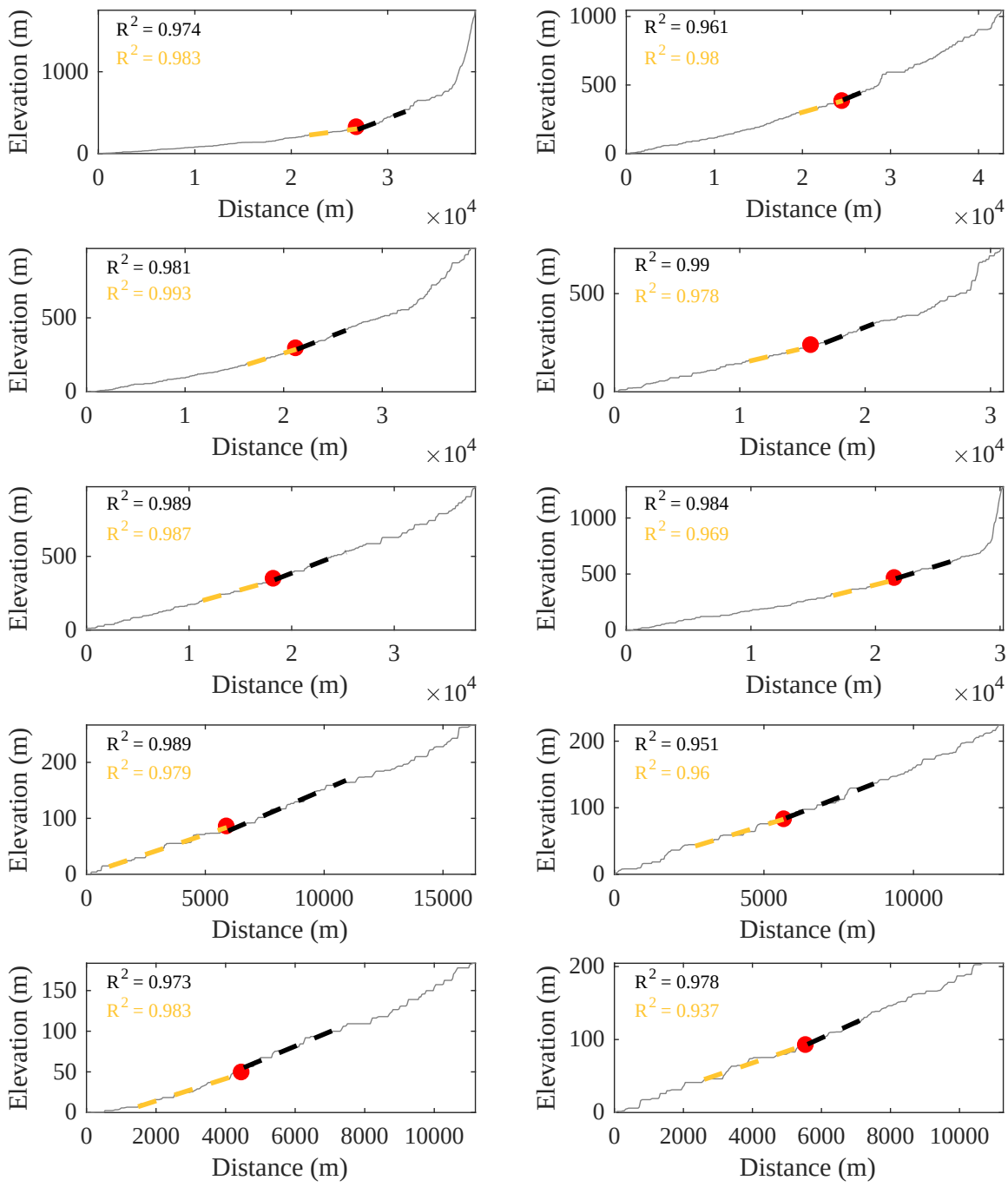

Figure DR13: Map, Digital Elevation Model and slope estimations of the 10 natural catchment-fan systems from the study site Suez (see Table 2). Grey line is the river profile, dotted lines indicate the linear fit in the foreland (orange) and in the catchment (black).

GSA DATA REPOSITORY

Guerit et al., Fluvial landscape evolution controlled by the sediment deposition coefficient: estimation from experimental and natural landscapes

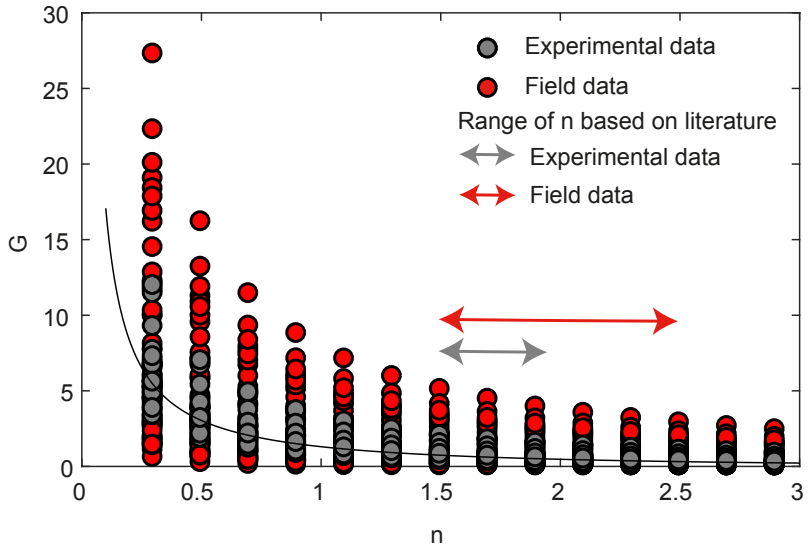

Figure DR14: Evolution of the deposition coefficient G as a function of the slope exponent n for experimental (gray dots) and field (red dots) data. The black line is the median G value and the arrows indicate the values of n that are used in this study, based on worldwide data set (DiBiase and Whipple, 2011; Whittaker, 2012; Lague, 2014; Harel et al., 2016). The data set is well-fitted by the empirical power law: $G = 1.6n^{-1.1}$.

References

DiBiase, R. A. and Whipple, K. X.: The influence of erosion thresholds and runoff variability on the relationships among topography, climate, and erosion rate, Journal of Geophysical Research: Earth Surface, 116, 2011.

Harel, M.-A., Mudd, S., and Attal, M.: Global analysis of the stream power law parameters based on worldwide 10Be denudation rates, Geomorphology, 268, 184–196, 2016.

Lague, D.: The stream power river incision model: evidence, theory and beyond, Earth Surface Processes and Landforms, 39, 38–61, 2014.

Whittaker, A.: How do landscapes record tectonics and climate?, Lithosphere, 4, 160–164, 2012.

GSA DATA REPOSITORY

Guerit et al., Fluvial landscape evolution controlled by the sediment deposition coefficient: estimation from experimental and natural landscapes

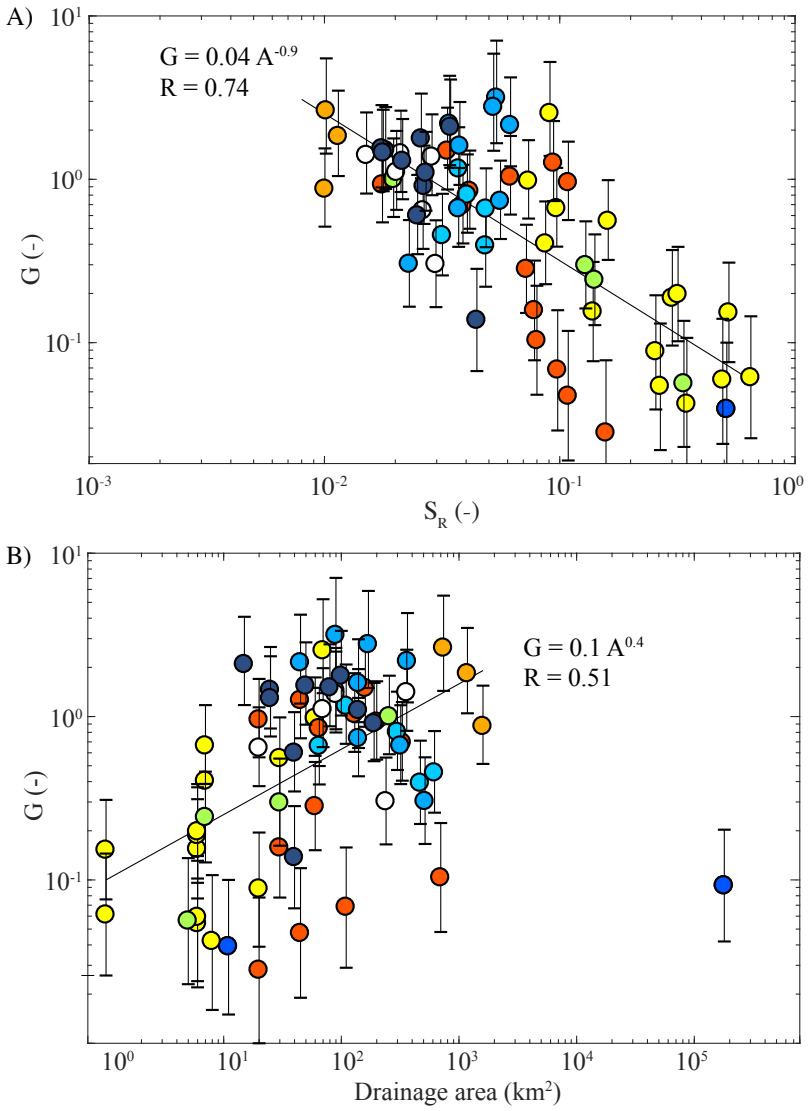

Figure DR15: Empirical relationships between the deposition coefficient G and A) the slope along the river in the range S_R, and B) the drainage area A. Errorbars account for uncertainties on n (see main manuscript). A correlation can be observed on both graphs, suggesting that steep and small catchments tend to have lower G. See Figures 2 and 4 for colorcode.

GSA DATA REPOSITORY

Guerit et al., Fluvial landscape evolution controlled by the sediment deposition coefficient: estimation from experimental and natural landscapes

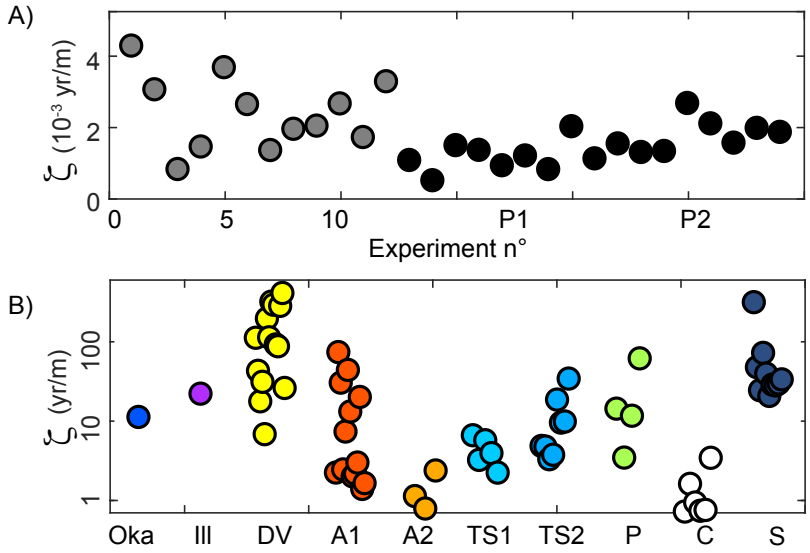

Figure DR16: Estimation of the scaling factor ζ for A) the experimental and B) the natural systems (note the logarithmic scale for the y-axis). See Figures 2 and 4 for colorcode.

GSA DATA REPOSITORY

Guerit et al., Fluvial landscape evolution controlled by the sediment deposition coefficient: estimation from experimental and natural landscapes

TABLE DR1. CHARACTERISTICS OF THE EXPERIMENTAL CATCHMENT-FAN SYSTEMS

Name	Uplift rate U	Precipitation rate P	Catchment area	Range slope S_R	Fan slope S_F	Deposition coeff. G	Scaling factor ζ
	(mm/h)	(mm/h)	(mm^2)	(-)	(-)	(-)	(yr/m)
Single fan-catchment system*							
1	5	80	24983	0.097	0.057	0.670	0.004
2	10	80	36181	0.137	0.070	0.470	0.003
3	5	40	57491	0.120	0.082	1.094	0.001
4	5	80	53548	0.126	0.084	0.995	0.001
5	5	130	35269	0.122	0.058	0.390	0.004
6	5	80	39769	0.152	0.082	0.544	0.003
7	2	80	66230	0.103	0.070	1.069	0.001
8	7	80	41815	0.133	0.080	0.740	0.002
9	3	80	66158	0.116	0.069	0.707	0.002
10	13	80	46648	0.130	0.070	0.540	0.003
11	5	80	49260	0.123	0.078	0.840	0.002
12	5	40	37895	0.166	0.106	0.875	0.003
Multiple fan-catchment system†							
P1	15	120	5379	0.161	0.104	0.901	0.001
			12764	0.129	0.101	1.945	0.001
			4247	0.193	0.112	0.646	0.001
			10780	0.168	0.100	0.710	0.001
			13350	0.132	0.089	1.047	0.001
			13299	0.132	0.082	0.804	0.001
			12356	0.122	0.085	1.189	0.001
P2	15	120	6622	0.196	0.101	0.475	0.002
			9947	0.135	0.086	0.863	0.001
			15644	0.167	0.095	0.626	0.002
			13909	0.145	0.088	0.743	0.001
			6019	0.154	0.093	0.727	0.001
			11682	0.170	0.078	0.359	0.003
			13217	0.166	0.084	0.457	0.002
			6548	0.147	0.083	0.617	0.002
			5421	0.158	0.082	0.486	0.002
			12526	0.164	0.087	0.516	0.002

* from Rohais (2007) and Rohais et al. (2012)

† from Babault et al. (2005)

REFERENCES CITED

Babault, J., Bonnet, S., Crave, A., and Van Den Driessche, J., 2005, Influence of piedmont sedimentation on erosion dynamics of an uplifting landscape: an experimental approach Geology, v. 33, no. 4, p. 301–304.

Rohais, S., 2007, Architecture stratigraphique et flux sédimentaires sur la marge sud du golfe de Corinthe (Grèce) : Analyse de terrain, modélisations expérimentales et numériques [Ph.D. thesis]: Université de Rennes 1, 386 p.

Rohais, S., Bonnet, S., and Echard, R., 2012, Sedimentary record of tectonic and climatic erosional perturbations in an experimental coupled catchment-fan system: Basin Research, v. 24, no. 2, p. 198–212.

GSA DATA REPOSITORY

Guerit et al., Fluvial landscape evolution controlled by the sediment deposition coefficient: estimation from experimental and natural landscapes

TABLE DR2. CHARACTERISTICS OF THE NATURAL CATCHMENT-FAN SYSTEMS

Name	Location		Precipitation rate P*	Area	Range slope S_R	Fan slope S_F	Deposition coeff. G	Scaling factor ζ
	Lat	Long	(mm/y)	(km^2)	(-)	(-)	(-)	(y/m)
Okavango (Botswana)	-18.7019	22.2143	1000	180000	$1.3\ 10^{-3}$	$0.4\ 10^{-3}$	0.092	11
Illgraben (Switzerland)	46.2881	7.6302	1200	11	0.513	0.099	0.039	21
Death Valley (US)	36.0572	-116.7568	60	6	0.139	0.051	0.154	108
	36.0588	-116.7450	60	7	0.087	0.047	0.402	41
	36.0683	-116.7367	60	60	0.074	0.052	0.974	17
	36.0822	-116.7160	60	30	0.161	0.096	0.553	30
	36.1337	-116.7486	60	70	0.091	0.077	2.527	7
	36.1525	-116.7664	60	20	0.256	0.073	0.088	189
	36.1670	-116.7621	60	1	0.524	0.190	0.152	110
	36.1849	-116.7610	60	6	0.268	0.060	0.054	309
	36.1930	-116.7626	60	6	0.493	0.116	0.059	282
	36.2113	-116.7648	60	6	0.301	0.119	0.187	89
	36.2265	-116.7624	60	6	0.318	0.129	0.197	85
	36.2403	-116.7654	60	1	0.649	0.156	0.061	273
	36.2601	-116.7720	60	8	0.347	0.069	0.042	397
	36.2856	-116.7867	60	7	0.097	0.061	0.661	25
Andes 1 (Argentina)	-29.5980	-67.1760	500	200	0.018	0.012	0.924	2
	-29.4980	-67.1906	500	20	0.157	0.026	0.028	71
	-29.4165	-67.1869	500	110	0.098	0.025	0.068	29
	-29.3326	-67.2348	500	65	0.041	0.028	0.844	2
	-29.2557	-67.2599	500	60	0.072	0.034	0.281	7
	-29.1699	-67.2892	500	45	0.109	0.023	0.047	43
	-29.0846	-67.3163	500	30	0.078	0.029	0.157	13
	-29.6512	-67.5306	500	130	0.062	0.044	1.031	2
	-29.5148	-67.5725	500	20	0.109	0.076	0.954	2
	-29.1457	-67.4963	500	330	0.039	0.025	0.691	3
	-29.0016	-67.4958	500	700	0.080	0.024	0.103	19
	-29.7485	-67.3721	500	160	0.033	0.026	1.487	1
	-29.6027	-67.5403	500	45	0.094	0.070	1.255	2

Andes 2 (Argentina)	-35.5444	-69.6006	500	1180	0.011	0.009	1.829	1
	-35.2102	-69.7026	500	740	0.010	0.009	2.624	1
	-34.9557	-69.7192	500	1600	0.010	0.007	0.870	2
Tian Shan 1 (Kazakhstan)	43.2597	77.2131	400	470	0.048	0.026	0.391	6
	43.3200	77.4955	400	300	0.041	0.027	0.800	3
	43.2906	77.6624	400	620	0.032	0.018	0.452	6
	43.4559	77.7390	400	65	0.049	0.031	0.657	4
	43.4562	77.8228	400	110	0.037	0.027	1.157	2
Tian Shan 2 (China)	41.9146	85.7000	100	45	0.062	0.051	2.133	5
	41.9865	85.5387	100	365	0.034	0.028	2.172	5
	42.0433	85.2651	100	90	0.054	0.047	3.138	3
	42.1209	85.0037	100	170	0.052	0.045	2.756	4
	42.0763	84.8633	100	320	0.037	0.023	0.660	15
	42.1813	84.7078	100	140	0.038	0.030	1.596	6
	42.0884	84.6330	100	140	0.056	0.037	0.733	14
	42.0184	84.5336	100	515	0.023	0.011	0.302	33
Pindus (Greece)	38.9036	22.1259	300	7	0.141	0.062	0.241	14
	38.8823	22.1641	300	256	0.020	0.014	0.997	3
	38.8762	22.2366	300	30	0.129	0.062	0.296	11
	38.8614	22.3213	300	5	0.337	0.078	0.056	60
Corinth Gulf (Greece)	38.2901	21.9850	1000	90	0.021	0.016	1.432	1
	38.2732	22.0247	1000	20	0.026	0.016	0.641	2
	38.2567	22.0527	1000	70	0.020	0.015	1.102	1
	38.2187	22.0750	1000	360	0.015	0.012	1.400	1
	38.1902	22.1499	1000	90	0.029	0.022	1.367	1
	38.1809	22.1934	1000	240	0.030	0.014	0.301	3
Suez Gulf (Egypt)	28.2555	33.8406	24	40	0.044	0.015	0.137	304
	28.2400	33.8702	24	190	0.027	0.018	0.904	46
	28.1480	33.8766	24	100	0.026	0.021	1.766	24
	28.1023	33.8982	24	40	0.025	0.015	0.597	70
	28.0801	33.9700	24	140	0.027	0.020	1.089	38
	28.0709	34.0144	24	15	0.034	0.028	2.082	20
	27.9512	34.0050	24	80	0.018	0.014	1.498	28
	27.8978	34.0612	24	50	0.018	0.014	1.536	27
	27.8742	34.0807	24	25	0.018	0.014	1.449	29
	27.8637	34.1224	24	25	0.022	0.016	1.288	32

* Data from: Wells et al. (1987); Geriesh et al. (2004); Jayko (2005); Wilk et al. (2006); Nikas et al. (2007); Metha et al. (2008); Chakraborty et al. (2010); Berger et al. (2011); Gessner et al. (2013); Zhao et al. (2014); Carretier et al. (2018).

REFERENCES CITED

Berger, C., McArdell, B., and Schlunegger, F., 2011, Sediment transfer patterns at the Illgraben catchment, Switzerland: Implications for the time scales of debris flow activities: Geomorphology, v. 125, no. 3, p. 421–432.

Carretier, S., Tolorza, V., Regard, V., Aguilar, G., Bermúdez, M., Martinod, J., Guyot, J.-L., Hérail, G., and Riquelme, R., 2018, Review of erosion dynamics along the major NS climatic gradient in Chile and perspectives: Geomorphology, v. 300, p. 45–68.

Chakraborty, T., Kar, R., Ghosh, P., and Basu, S., 2010, Kosi megafan: Historical records, geomorphology and the recent avulsion of the Kosi River: Quaternary International, v. 227, no. 2, p. 143–160.

Geriesh M., El-Rayes A., and Fouad A., 2004, Runoff control and water management in Wadi Ghweabae hydrographic basin, Northwest of Gulf of Suez region, Egypt: Proc. 7th Conf. Geology of Sinai for Development, Ismailia, p. 53–67.

Gessner, U., Naeimi, V., Klein, I., Kuenzer, C., Klein, D., and Dech, S., 2013, The relationship between precipitation anomalies and satellite-derived vegetation activity in Central Asia: Global and Planetary Change, v. 110, p. 74–87.

Jayko, A., 2005, Late Quaternary denudation, Death and Panamint valleys, eastern California: Earth-Science Reviews, v. 73, no. 1-4, p. 271–289.

Mehta, A., and Yang, S., 2008, Precipitation climatology over Mediterranean Basin from ten years of TRMM measurements: Advances in Geosciences, v. 17, p. 87–91.

Nikas, K., Antonakos, A., Lambrakis, N., and Kallergis, G., 2007, The use of antecedent precipitation index and delay factor to estimate runoff from rainfall: A case study from eight drainage basins-Achaia, Peloponessos, Greece: Bulletin of the Geological Society of Greece, v. 37.

Wells, N., and Dorr Jr, J., 1987, Shifting of the Kosi river, northern India: Geology, v. 15, no. 3, p. 204–207.

Wilk, J., Kniveton, D., Andersson, L., Layberry, R., Todd, M., Hughes, D., Ringrose, S., and Vanderpost, C., 2006, Estimating rainfall and water balance over the Okavango River Basin for hydrological applications: Journal of Hydrology, v. 331, no. 1-2, p. 18–29.

Zhao, Y., Huang, A., Zhou, Y., Huang, D., Yang, Q., Ma, Y., Li, M., and Wei, G., 2011, Impact of the middle and upper tropospheric cooling over central Asia on the summer rainfall in the Tarim Basin, China. Journal of Climate: v. 27, no. 12, p. 4721–4732.